J. Fluid Mech. (1993), *vol.* 247, *pp.* 455–488

Mode interaction models for near-wall turbulence

By SANJEEV SANGHI† AND NADINE AUBRY

The Benjamin Levich Institute and Department of Mechanical Engineering, City College of the City University of New York, NY 10031, USA

(Received 4 January 1992)

Intermittent bursting events, similar to those characterizing the dynamics of near-wall turbulence, have been observed in a low-dimensional dynamical model (Aubry *et al.* 1988) built from eigenfunctions of the proper orthogonal decomposition (Lumley 1967). In the present work, we investigate the persistency of the intermittent behaviour in higher- but still of relatively low-dimensional dynamical systems. In particular, streamwise variations which were not accounted for in an explicit way in Aubry *et al.*'s model are now considered. Intermittent behaviour persists but can be of a different nature. Specifically, the non-zero streamwise modes become excited during the eruptive events so that rolls burst downstream into smaller scales. When structures have a finite length, they travel at a convection speed approximately equal to the mean velocity at the top of the layer ($y^+ \approx 40$). In all cases, intermittency seems to be due to homoclinic cycles connecting hyperbolic fixed points or more complex (apparently chaotic) limit sets. While these sets lie in the zero streamwise modes invariant subspace, the connecting orbits consist of non-zero streamwise modes travelling downstream. Chaotic limit sets connected by quasi-travelling waves have also been observed in a spatio-temporal chaotic regime of the Kuramoto–Sivashinsky equation (Aubry & Lian 1992*a*). When the limit sets lose their steadiness, the elongated rolls become randomly active, as they probably are in the real flow. A coherent structure study in our resulting flow fields is performed in order to relate our findings to experimental observations. It is shown that streaks, streamwise rolls, horseshoe vortical structures and shear layers, present in our models, are all connected to each other. Finally, criteria to determine a realistic value of the eddy viscosity parameter are developed.

1. Introduction

Despite the contribution of many researchers, the mechanism of turbulence production in near-wall turbulence is still poorly understood. However, it seems well established that a large fraction of the production occurs during violent explosions (or 'bursts') of otherwise quiescent streamwise streaks (see for example Cantwell 1981). Streaks, visualized by Kline *et al.* (1967) using hydrogen bubbles, have been associated with streamwise rolls (Bakewell & Lumley 1967; Blackwelder & Eckelman 1979; Kim 1985; Adrian, Moin & Moser 1987; Moin & Moser 1989). The structure of near-wall turbulence has received considerable interest and significant progress has recently been achieved with the generation of highly detailed numerical simulation data (Moin & Kim 1982; Spalart 1988). Nevertheless, the complexity of the data has

† Present address: Department of Applied Mechanics, Indian Institute of Technology, New Delhi 110016, India.

made their interpretation extremely difficult in terms of coherent structures and their dynamics (see e.g. the detailed kinematical study of Robinson, Kline & Spalart 1990 who analysed Spalart's 1988 numerical data). It has recently become obvious that there is a need for simplified numerical simulations and models. Examples of such models are those of Jimenez *et al.* (1988), Landahl (1990) and Jimenez & Moin (1990). In the latter, the authors carry out an extremely reduced simulation in which the spanwise periodic length is about 100 wall units (i.e. the average distance between two streaks) so that one streak can be isolated and studied in detail. The striking result of their study is that this course simulation generates approximately correct first- and second-order statistics.

Another simplified model is that of Aubry *et al.* (1988) who derive a set of ten ordinary differential equations (referred to as the 10D model below) for the dynamics of infinitely long streamwise rolls in a spanwise periodic box of 333 wall units, over a vertically bounded domain of 40 wall units. Not only can the rolls, extracted from experimental two-point correlations via the proper orthogonal (or Karhunen–Loève) decomposition, reproduce approximately correct statistics, but they also exhibit interesting intermittent dynamics whose nature resembles that of the bursting event experimentally observed. In dynamical systems terminology, these cyclic dynamics are due to the presence, in phase space, of an attracting heteroclinic cycle connecting two hyperbolic fixed points, or saddle points. The solution spends a relatively long time near one of the (unstable) steady solutions, oscillates and suddenly bursts through a brief jump to another quiescent state, only translated in the cross-stream direction with respect to the first one. In physical space streamwise rolls, quiescent for a long time, start to oscillate, suddenly burst and re-form. Although, formally, the interburst time keeps increasing as the solution approaches the (attracting) heteroclinic cycle (on which a fixed point can be reached only after an infinitely long time), the presence of noise or 'external' forcing equilibrates the time occurrence of the eruptive events. (A main source of noise in Aubry *et al.*'s 1988 model is identified with the external-layer jitter which enters the dynamical system as the fluctuating pressure term at the upper boundary.) Then, the dynamics repeats itself an infinite number of times, consistently with the bursting event viewed as a cycle, including both the secondary instability mechanism and the roll reformation. Although the presence of heteroclinic cycles has not yet been identified in experimental data, the distribution of bursting events has been observed to display exponential tails (Kim, Kline & Reynolds 1971; Bogard & Tiederman 1986) which is, as shown by Stone & Holmes (1989, 1990), characteristic of saddle–saddle connections in the presence of external random or regular forcing.

Following this pioneering work, a number of studies related to heteroclinic cycles appeared. The first was that of Guckenheimer & Holmes (1988) who addressed the intriguing issue of the stability of heteroclinic cycles, which are known to be unstable to small perturbations (see e.g. Guckenheimer & Holmes, 1983). They showed that saddle–saddle connections can be stabilized by the presence of symmetries, as is obviously the case in Aubry *et al.*'s (1988) study in which the relevant symmetry group is $O(2)$, consisting of (statistical) spanwise reflections and translations.† Indeed, heteroclinic cycles in the presence of symmetries have been observed by Busse & Heikes (1980) in a convective rotating layer, Proctor & Jones (1988) in a two-mode model of Bénard convection and Hyman, Nicolaenko & Zaleski (1986) in

† 'Statistical symmetry' refers to a property of the statistics of the flow, in particular the two-point correlation tensor. While the equations of motion are also invariant under the symmetry, the *instantaneous* flow, at a given time, in general, is not.

the numerical solutions of the Kuramoto–Sivashinsky equation with periodic boundary conditions. The existence and stability of such solutions in the context of Aubry *et al.*'s (1988) boundary-layer study was proved by Armbruster, Guckenheimer & Holmes (1988) for a 4D model (a subset of the 10D model described above). Later, it was shown by Campbell & Holmes (1991) that heteroclinic cycles still exist in a 6D model and become unstable to travelling and modulated travelling waves. Recently, saddle–saddle connections have been discovered in many fluid flow systems. For example, Nicolaenko & She (1992) observe a bursting mechanism based on symmetry-equivariant cycles (the symmetry involved is $SO(2) \times D_k$) in two-dimensional Kolmogorov flows, Leibovich & Mahalov (1993) show numerical evidence of heteroclinic connections in several $SO(2)$-equivariant (i.e. translation invariant) systems modelling wave interactions among invariant subspaces of the Navier–Stokes equations, and Mullin & Darbyshire (1989) demonstrate the presence of heteroclinic and homoclinic cycles in an $SO(2)$-equivariant Taylor–Couette apparatus with rotating endplates. Finally, we should mention the 'heteroclinic connections to infinity' which connect a finite part of the phase space to infinity of Newell, Rand & Rusell (1988) and represent the principal contributor to the dissipation rate.

As far as the importance of heteroclinic cycles for the near-wall dynamics is concerned, an open issue in Aubry *et al.*'s (1988) work, which we address in this paper, is the robustness of the proposed intermittency mechanism to the order of truncation, as one knows that the behaviour of a finite- or low-dimensional dynamical system may be a mere artifact of the truncation (see e.g. Curry 1978; Curry *et al.* 1984 regarding Lorenz's model as an approximation to the Boussinesq equations). Although one may argue that symmetry-induced phenomena should persist at any resolution which preserves the symmetries, such an assertion concerning intermittency is worth investigating. Moreover, as recalled above, streamwise variations, which are obviously important in a fully developed, turbulent flow are neglected in Aubry *et al.*'s (1988) model. They may have a crucial role in a more complete resolution, as they impose, for instance, new symmetries to the system, namely an $SO(2)$-invariance due to the streamwise homogeneity of the flow. For example, propagation of the flow patterns downstream is certainly a consequence of this symmetry; the question is then: Can intermittency and propagation co-exist? If yes, how is intermittency modified by propagation?

The paper is organized as follows. We recall the equations of motion for the boundary-layer flow in the next section, and the results from the 10D model of Aubry *et al.* (1988) in §3. In §4, we discuss the necessity of adding non-zero streamwise modes. In §5, we analyse the set of equations for any number of modes in terms of invariant subspaces and their relation to the statistical symmetries of the flow. The results of the integration of 32-, 54- and 64-dimensional models (including up to six spanwise, three streamwise and two normal modes) are presented in §6. In §7, we extract the physical 'coherent' structures from the flow fields thus obtained and show that low-speed streaks, ejections, sweeps, horseshoe vortical structures and near-wall shear layers, observed in experimental studies, are all present in our models. Finally, criteria to deduce a realistic value for the eddy viscosity parameter, used in the Heisenberg model to represent the action of unresolved scales onto resolved modes, are developed and investigated in §8.

Although some preliminary results from this study were described in earlier publications (Aubry & Sanghi 1989, 1991; Sanghi & Aubry 1991), many further details are given in this paper.

2. Equations of motion

We recall in this section the modelling of the flow by deriving sets of ordinary differential equations from the Navier–Stokes equations (Aubry 1987; Aubry *et al.* 1988).

2.1. *The proper orthogonal decomposition*

The model uses the proper orthogonal decomposition (POD) (Loève 1955) – also called the Karhunen–Loève expansion or principal component analysis – which was introduced and developed in turbulence by Lumley (1967, 1970, 1981) to identify coherent structures in a random flow. Specifically, the technique extracts deterministic functions $\phi^{(n)}(x)$ from a set of realizations $\boldsymbol{u}_\omega(x)$ of an energy-integrable random velocity field such that

$$\int R(x,x')\,\phi^{(n)}(x')\,\mathrm{d}x' = \lambda^{(n)}\phi^{(n)}(x), \tag{1}$$

where $R(x,x')$ is the autocorrelation matrix $\langle \boldsymbol{u}_\omega(x)\,\boldsymbol{u}_\omega(x')\rangle_\omega$ (the angle brackets denoting the ensemble average over various realizations ω). A significant feature of the decomposition, used as a partial justification for a truncation of dynamical systems based on such modes, is the fact that the convergence is optimally fast in quadratic mean, the eigenvalues being ordered in a decreasing manner $\lambda^{(1)} \geqslant \lambda^{(2)} \geqslant \ldots$. Under the assumption of the ergodicity of the flow (often made if the flow is statistically stationary) (Aubry *et al.* 1988; Sirovich 1987), one can substitute the ensemble average by the time average and put the time information in the coefficients $a^{(n)}$ of the expansion. This assumption, as well as the energy integrability of the flow (recall that there is no proof of the energy integrability of three-dimensional flows) is not needed if one considers deterministic decompositions of functions defined on a space–time domain $X \times T$ (Aubry, Guyonnet & Lima 1991, 1992*b*; Aubry 1991) into orthonormal functions in a Hilbert space $H(T)$ and orthonormal functions in a Hilbert space $H(X)$. These *biorthogonal* decompositions are useful tools for the treatment of spatio–temporal dynamical systems (Aubry, Guyonnet & Lima 1991, 1992*a*; Aubry & Lian 1992*a*; Slimani *et al.* 1992).

The three-dimensional shear flow of the wall region is considered homogeneous in the streamwise (x_1 or x) and spanwise (x_3 or z) directions, stationary in time and inhomogeneous in the normal direction (x_2 or y). As is common in numerical simulations, we restrict our study to a periodic box in the x_1 and x_3 directions, of size $L_1 \times L_3$. In this case, it is well-known (Lumley 1967) that the proper orthogonal modes factorize into Fourier modes in the two homogeneous directions x_1 and x_3 and (eigen)functions in the normal direction x_2. The velocity field fluctuation is then expanded as

$$u_i(x_1,x_2,x_3,t) = \frac{1}{(L_1 L_3)^{\frac{1}{2}}} \sum_n \sum_{l,k} a_{lk}^{(n)}(t)\,\mathrm{e}^{2\pi\mathrm{i}(lx_1+kx_3)}\phi_{i_{lk}}^{(n)}(x_2), \tag{2}$$

where l, k are the streamwise and spanwise wavenumbers (u_1, u_2, u_3 also denoted u, v, w below). The eigenfunctions $\phi_{\boldsymbol{k}}^{(n)}$, $\boldsymbol{k}$ representing the vector (l,k), are extracted from the equation

$$\int \Phi_{ij_k}(x_2,x_2')\,\phi_{j_k}^{(n)}(x_2')\,\mathrm{d}x_2' = \lambda_{\boldsymbol{k}}^{(n)}\,\phi_{i_k}^{(n)}(x_2), \tag{3}$$

where Φ_{ij} denotes the Fourier transform of the autocorrelation tensor in the x_1, x_3 directions at zero time lag: $R_{ij}(x_1-x_1', x_2, x_2', x_3-x_3')_{t-t'=0}$. Further details can be found

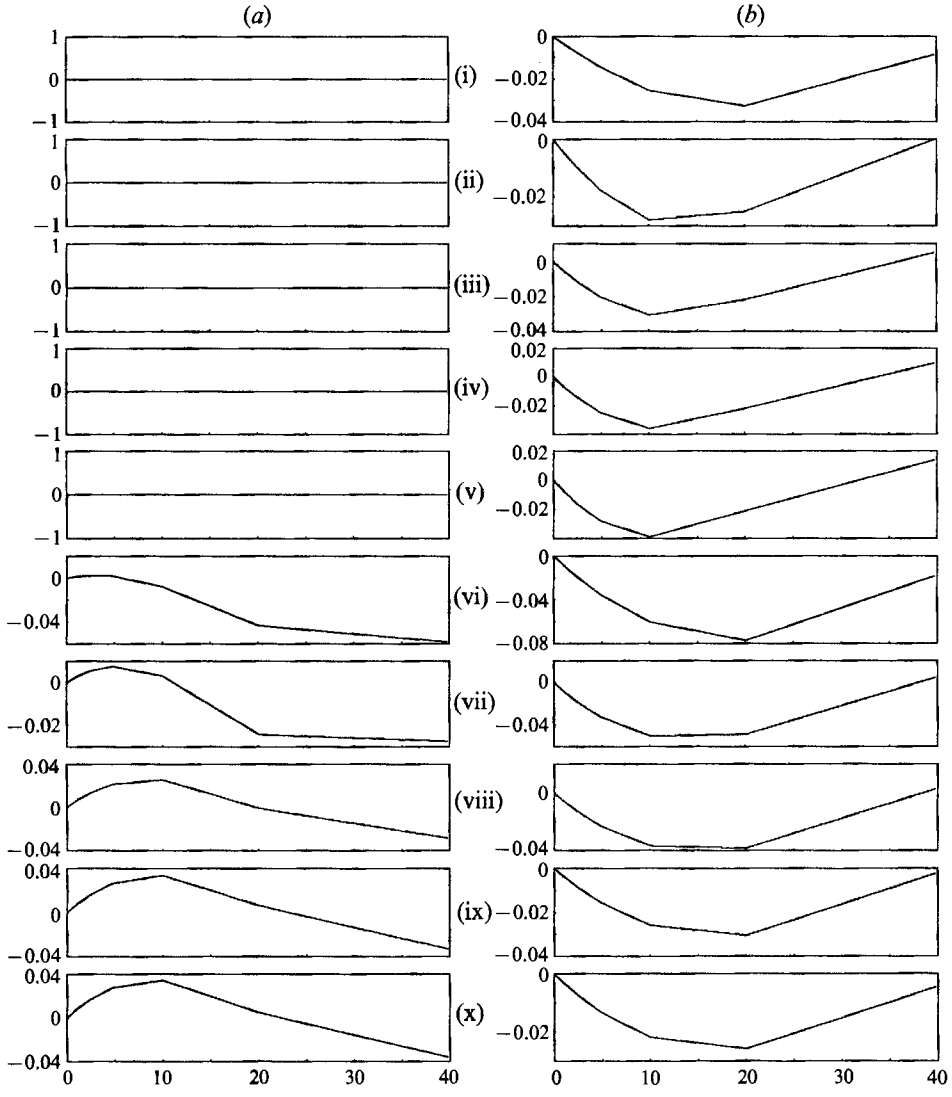

FIGURE 1. Real (a) and imaginary (b) parts of the first component of the POD eigenfunctions as functions of x_2 for different wave vectors $\boldsymbol{k}$: (i) $(0, 3\times10^{-3})$; (ii) $(0, 6\times10^{-3})$; (iii) $(0, 9\times10^{-3})$; (iv) $(0, 1.2\times10^{-2})$; (v) $(0, 1.5\times10^{-2})$; (vi) $(1.5\times10^{-3}, 3\times10^{-3})$; (vii) $(1.5\times10^{-3}, 6\times10^{-3})$; (viii) $(1.5\times10^{-3}, 9\times10^{-3})$; (ix) $(1.5\times10^{-3}, 1.2\times10^{-2})$; (x) $(1.5\times10^{-3}, 1.5\times10^{-2})$ from the experimental data of Herzog (1986).

in Aubry *et al.* (1988). Let us only recall here, as it will be useful in §8, that the eigenfunctions are orthogonal:

$$\int \phi_{i_k}^{(n)} \phi_{i_{k'}}^{(m)*} \, \mathrm{d}x_2 = \delta_{nm} \, \delta_{kk'}, \tag{4}$$

and that the time-dependent coefficients $a_k^{(n)}(t)$ are uncorrelated (the angle brackets denote the ensemble average, identified here with the time average):

$$\langle a_k^{(n)} \, a_{k'}^{(m)*} \rangle = \lambda_k^n \, \delta_{mn} \, \delta_{kk'}. \tag{5}$$

As in Aubry *et al.* (1988), the flow investigated is the wall region ($0 < x_2^+ < 40$) of

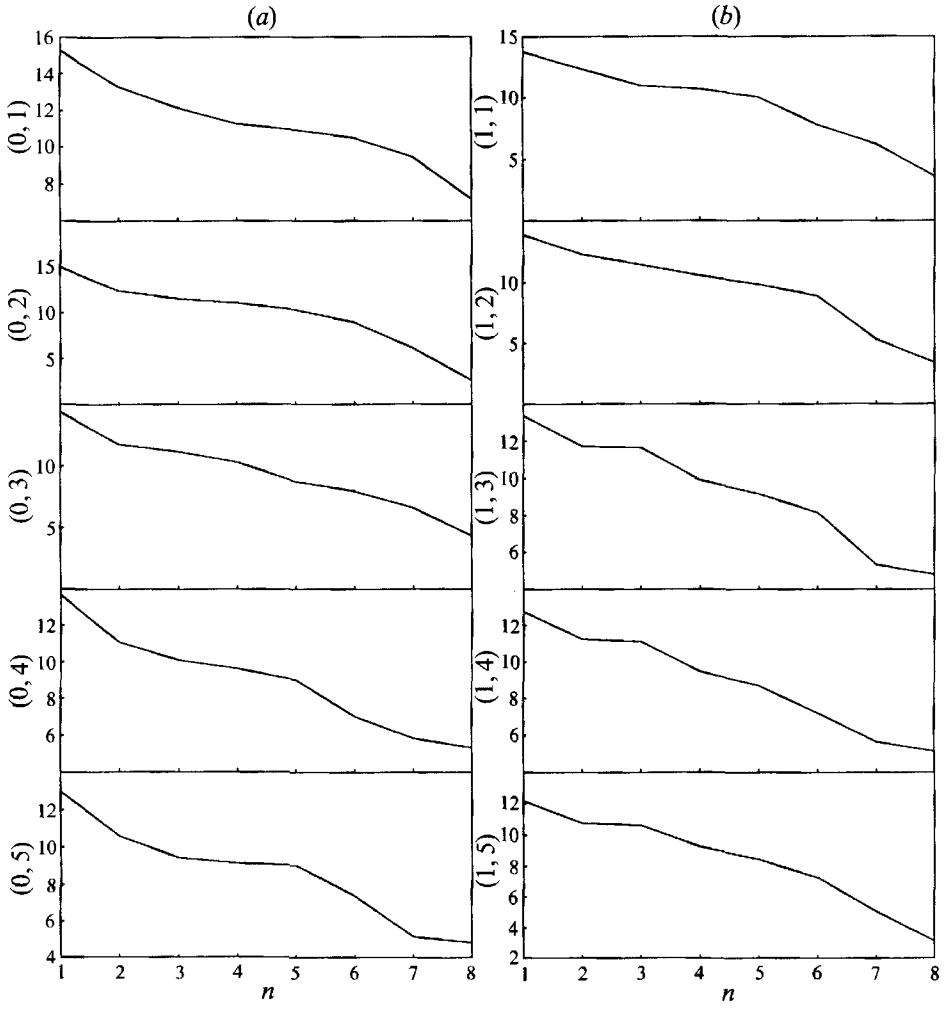

FIGURE 2. $\ln \lambda_{l,k}^{(n)}$ as a function of n for different wave vectors (l, k) from the experimental data of Herzog (1986). The spanwise wavenumbers are the same as in figure 1; (*a*) $l = 0$, (*b*) $l = 1.5 \times 10^{-3}$.

a pipe flow (Herzog 1986) of Reynolds number 8750, based on the centreline mean velocity and the diameter of the pipe. Figure 1 displays selected functions $\phi_{i_k}^{(1)}(x_2)$ and figure 2 the energy spectrum $\lambda_k^{(n)}$ versus n for various wavenumber pairs $\boldsymbol{k} = (k_1, k_3)$. It is interesting to note that spectra tend to decay exponentially fast, which justifies the severe truncations in the normal direction ($n = 1$ in Aubry *et al.* 1988 and $n = 1, 2$ in this paper). This also indicates that there may exist a self-similarity among the modes, due to the existence of a spatio–temporal symmetry (Aubry *et al.* 1992*a*, *b*; Aubry & Lian 1992) which will be investigated in future work. We have carried out integrations of dynamical equations whose coefficients have been computed from the database generated by the direct numerical simulation of turbulent channel flow of Kim, Moin & Moser (1987) at a Reynolds number of 6600, based on the mean centreline velocity and channel width. Since we get similar results in both cases, we shall present those obtained from the experimental data only.

2.2. *The equations of motion*

The general dynamical equations are the same as in Aubry *et al.* (1988, Appendix A) and are obtained by a Galerkin projection of the Navier–Stokes equations onto the POD eigenmodes $\phi_k^{(n)} e^{2\pi i l x}$ (x representing the vector (x_1, x_3)) expanding the fluctuating field only. They consist of sets of ordinary differential equations (ODEs):

$$L\frac{da_k^{(n)}}{dt} = \sum_m b_k^{(n)(m)} a_k^{(m)} + \sum_{pqk'} c_{kk'}^{(n)(p)(q)} a_{k'}^{(p)} a_{k-k'}^{(q)} + \sum_{pqrk'} d_{kk'}^{(n)(p)(q)(r)} a_{k'}^{(r)} a_{k'}^{(p)} a_k^{(q)*} - \phi_{2_k}^{(n)*} \hat{p}_k(t), \tag{6}$$

where $L = (L_1 L_3)^{\frac{1}{2}}$, including linear, quadratic and cubic terms whose coefficients are recalled in Appendix A. The quadratic terms represent the energy transfer between the different eigenmodes, while the cubic terms, resulting from the interaction between the Reynolds shear stress and the fluctuation (see equation (15) in Aubry *et al.* 1988), control the amplification of the structures by weakening the mean velocity profile as the fluctuation grows. Although the pressure term in (6) (the hat denotes the Fourier transform in the x_1, x_3 directions) usually disappears in Galerkin projections, its contribution from the upper boundary ($X_2^+ = 40$) remains due to the restriction of our study to the wall region. Nevertheless, since this term is small and its action on intermittent dynamics is clearly understood (see the introduction) it is henceforth omitted. When streamwise variations are considered, the term $u_{i,1} U$ in the Navier–Stokes equations introduces extra linear and cubic terms in the ODEs representing the downstream propagation of the flow.

Since the set of ODEs (6) is necessarily truncated, the energy transfer to the unresolved scales is represented by a simple generalization of the Heisenberg spectral model as it is commonly used with success in large-eddy numerical simulations. The Reynolds stress tensor of the unresolved scales is assumed proportional to the strain rate tensor of the resolved scales:

$$\tau_{ij>} \propto -\nu_T (u_{i<,j} + u_{j<,i}), \tag{7}$$

where $>$ and $<$ represents the unresolved modes. ν_T is an approximate transport coefficient (eddy viscosity) proportional to the product of the characteristic lengthscale, $l_>$, and the velocity scale, $u_>$, of the unresolved modes:

$$\nu_T = \alpha u_> l_>. \tag{8}$$

The coefficient α is referred to as the Heisenberg parameter and its value determines the magnitude of the energy loss to the unresolved modes. This representation changes, on the one hand, the linear terms by a modified viscosity, and, on the other hand, the quadratic terms by the addition of a small pseudo-pressure term.

Sirovich, Ball & Keefe (1990) analyse Keefe, Moin & Kim's (1987) numerical simulation of a turbulent channel flow at Reynolds number 3000 (based on the channel width) using the proper orthogonal decomposition. Since the full velocity field $u(x, t)$ was available (on a coarse grid), they extract both the eigenmodes and the time-dependent coefficients. Their main finding is that all zero streamwise wavenumber modes are non-propagating modes while all non-zero streamwise wavenumber modes propagate. We will comment more on these results in §6. More recently, Zhou & Sirovich (1992) derived dynamical systems for the wall region, based on the previous full channel POD modes which are *linearly* mapped to those of the wall region. Although their motivation is to cancel the pressure term at the

upper edge of the layer, they have to input the two-point correlation tensor for the whole channel. In addition, the existence of a *linear* mapping when a finite number of modes is involved needs further investigation (for further comments, see Berkooz *et al.* 1992). Selecting the same truncation as in Aubry *et al.* (1988), they recover the basic intermittency mechanism which was however lost as they added a non-zero streamwise mode.

3. Results of the integration of the ten-dimensional model

In Aubry *et al.*'s (1988) study, the expansion of the velocity field is severely truncated to the first eigenmode ($n = 1$), six (positive) spanwise Fourier modes with a periodic cross-stream box length of $L_3^+ = 333$ wall units and the zero streamwise Fourier mode. This led to the 10D model discussed above, which is invariant under the action of the $O(2)$ symmetry group as a consequence of the statistical invariance of the boundary-layer flow in its turbulent stage under spanwise translations and reflections. It is interesting to note that a finite-dimensional Galerkin projection of a partial differential equation (PDE) onto POD eigenmodes does not necessarily preserve the symmetries of the original PDE. This problem can be solved by involving an average over the symmetry group in the decomposition technique (1), a procedure proposed by Aubry, Lian & Titi (1993) for this purpose. In the present study, we do not encounter this difficulty since the symmetries are systematically preserved because they are inherent to the Fourier components of the eigenmodes. This remark is still valid with the inclusion of downstream variations, which introduces streamwise symmetries (see below).

We now recall typical solutions observed in the 10D model (Aubry *et al.* 1988) since similar, but more complicated, behaviour will appear in higher-dimensional models. For $\alpha > 2.41$, the zero fixed point (steady solution) is the global attractor. For $2.3 < \alpha < 2.41$ and $1.61 < \alpha < 2.3$, there is a circle (namely an S^1-family due to the translation symmetry) of attracting fixed points in the even spanwise Fourier mode (2/4) subspace. Each fixed point represents two pairs of steady counter-rotating streamwise rolls in the periodic box of length $L_3^+ = 333$ which correspond to streaks of slow fluid going away from the wall. For α between 1.3 and 1.61, the fixed points destabilize and intermittent solutions appear. These belong to an S^1-symmetric family of heteroclinic cycles connecting saddle points which are out of phase on the circle of fixed points by π. A similar window of heteroclinic bursting solutions exists for values of α lying between 2.0 and 2.3, but this type of intermittency is simpler, involving no oscillatory motions in the unstable directions of the fixed points. From here on, we refer to this window of intermittency as window I and to the previous one as window II. For α between 1.0 and 1.3, the system displays a complex behaviour possibly including chaotic motions. When α decreases below 1.0, modulated travelling waves and travelling waves are observed, representing rolls propagating across the flow.

In previous studies, the expansion was truncated to the zero streamwise Fourier mode, hence preventing any x_1 dependence of the velocity and pressure, based on the experimental observation that the main structures of the flow (streaks) are elongated streamwise patterns. Paradoxically, this does not represent a fluid flow with no streamwise variations, i.e. a solution of the Navier–Stokes equations with $\partial/\partial x_1 = 0$. If this were the case, then as pointed out by Moffatt (1990), the streamwise velocity component would decouple from the spanwise and normal components and turbulence would simply decay. It turns out that, since the real flow is three-

dimensional, the eigenmodes, in particular those corresponding to $n = 1$ and zero streamwise wavenumber, keep track of this three-dimensionality and lead to a reasonable approximation of the Reynolds shear stress $\langle u_1 u_2 \rangle$ in the wall region. The latter, indeed, is different from zero as both components ϕ_1, ϕ_2 keep the same sign across the layer, independently of the cross-stream wavenumber (Aubry *et al.* 1988). This is also the reason why cubic coefficients in the ODEs are all negative, making the attractor globally stable, and why the turbulence production term remains positive, maintaining the fluctuation alive. As noticed by Berkooz, Holmes & Lumley (1991), this is equivalent to a closure assumption. However, a striking feature of the model is that, even if one forces the streamwise and cross-stream fluctuations to evolve independently by decoupling the eigenfunctions $(\phi_{1_k}, \phi_{2_k}, \phi_{3_k})$ into $(\phi_{1_k}, 0, 0)$ and $(0, \phi_{2_k}, \phi_{3_k})$, the turbulence decays in an intermittent fashion (Berkooz *et al.* 1991).

4. Deficiency of the ten-dimensional model

Although the 10D model could reproduce many of the qualitative phenomena experimentally observed in the dynamics of coherent structures in the wall region, the representation was rudimentary and limited in several ways. There is no doubt that more modes than those retained in this first model are dynamically active in the real flow and the question is to investigate how these extra scales modify the basic intermittency. *A priori*, the crudest approximation in the 10D model originates in the lack of streamwise variations, as we now discuss.

A weakness of the zero streamwise mode model is that it does not reproduce the right distribution of energy among the three components, as compared with the real flow. Too much energy is contained in the streamwise component. A detailed study has been performed by Aubry (1987) to examine the supply of energy as extra modes are added. It is shown there that the first eigenmode ($n = 1$) retains at least 65% of the energy in all three directions. We are more concerned about the truncation of the Fourier series. Reduction from 17 to 6 spanwise modes within the same periodic cell does not make a significant difference across the whole layer. However, addition of other streamwise wavenumbers (even one) helps considerably in recovering a more correct energy distribution and the best repartition is obtained when the streamwise length L_1 is 666 wall units.

In addition, physical phenomena such as the downstream convection of finite-length structures and the possibility of streamwise instabilities should lead to some interesting phenomena during the bursts.

5. Properties of the ODEs

The set of dynamical equations for the general case are given in Aubry *et al.* (1988). The properties of the ODEs truncated with one eigenmode ($n = 1$), any number N_1 of positive streamwise Fourier modes: $0, K_1, 2K_1, \ldots (N_1 - 1)K_1$ and any number N_3 of positive spanwise Fourier modes: $0, K_3, 2K_3, \ldots (N_2 - 1)K_3$ are discussed in this section.

5.1. *Complexity due to the presence of non-zero streamwise wavenumbers*

The addition of more streamwise modes makes the system much more complex. First, it increases the number of unknowns. The fact that the velocity field is real implies that $a_k^{(n)}(t)$ and $a_{-k}^{(n)}(t)$ are related and thus we do not consider the equations

for $a_{l,-k}$ (k non-negative) (where we have dropped the superscript (1) denoting $n = 1$). Nevertheless, every extra streamwise Fourier mode l (and of course its counterpart $-l$) adds not only the modes $a_{l,k}$ (with $l > 0$) but also $a_{-l,k}$. Consequently, the number of new complex unknowns included in the system by addition of an extra mode l is $2N_3 - 1$ (not just N_3), where N_3 is the number of resolved positive spanwise modes. A system including N_1 streamwise modes contains $N_3(2N_1 - 1) - N_1$ (that is 16 for $N_1 = 2$, $N_3 = 6$) complex equations.

In a zero streamwise mode model, owing to symmetry properties of the two-point correlation tensor at zero time lag, the components of the eigenfunctions are either real or imaginary which makes all the coefficients of the equations real. This is no longer the case when streamwise variations are included.

The addition of streamwise Fourier modes introduces relations among some of the coefficients of the differential equations. These symmetries are essential for the properties of the equations, leading to the invariance of the ODEs under the action of the $O(2) \times SO(2)$ symmetry group, consisting of spanwise translations and reflections (as in the 10D model) and streamwise translations. They are the direct consequence of the symmetries of the eigenfunctions and therefore come from the properties of the autocorrelation tensor, which are due to the fact that the flow itself satisfies statistically the symmetries of the Navier–Stokes equations (subject to the wall boundary conditions). Such relations were derived in Aubry (1987) and are not reproduced here; they sometimes involve up to 108 terms.

5.2. *Properties of the equations*

The general properties of the equations derived for a system truncated to $n = 1$ including any number of streamwise and spanwise Fourier modes are described in Aubry (1987). Because of their considerable importance to the types of solutions observed, they are briefly recalled here.

The contribution to the turbulence production of all Fourier mode pairs (l, k) of the first eigenmode ($n = 1$) is positive according to the experimental data. This positive contribution is due to the opposite signs of the streamwise and normal components of the first eigenmode. This has two consequences: First, the real part of the linear term originating from the mean pressure gradient is positive and represents a supply of energy from the mean flow. Second, the Reynolds shear stress is negative and therefore the real parts of the cubic coefficients are also negative, which guarantees the global stability of the solution. As in the 10D model, this reflects that, for the streamwise elongated vortices represented by the term $n = 1$, the mean flow stabilizes the perturbation as it grows and, conversely, the growing perturbation reduces the mean velocity gradient.

The ODEs have several important invariant subspaces which are very general and come from the intrinsic nature of the equations, regardless of the number of spanwise and streamwise wavenumbers. Since both the linear and cubic terms involve $a_{l,k}$, these terms are irrelevant to the existence of the invariant subspaces.

The first invariance reflects the property of homogeneity of the flow in the spanwise and streamwise directions, that is the statistical invariance under translation in these two directions. The ODEs are invariant under the transformation: $a_{lk} \to a_{lk} e^{i(l\theta + k\alpha)}$.

Second, the zero streamwise wavenumber subspace $l = 0$ is an invariant subspace. If a variable $a_{l,k} (l \neq 0)$ is initially zero, it remains zero since the triplet $(l \neq 0, l' = 0, l'' = 0)$ does not constitute an interacting triad. This subspace is $2(N_3 - 1)$ (that is 10 for $N_3 = 6$) dimensional. Similarly, we can use the same argument

to show that the subspace $k = 0$ is an invariant $2(N_1 - 1)$ (that is 2 for $N_1 = 2$) dimensional subspace.

Other important subspaces are the k-even subspace and the l-even subspace, which can be seen by considering a triad (Aubry 1987). An even mode initially zero can be excited by non-zero odd modes, making the odd subspace non-invariant while odd modes, initially zero, will remain zero, making the even subspace invariant. The dimension of the k-even subspace is $2((2N_1 - 1)[\frac{1}{2}(N_3 + 1)] - N_1)$ (that is 14 for $N_1 = 2$, $N_3 = 6$) while the dimension of the l-even subspace is $2((2[\frac{1}{2}(N_1 + 1)] - 1)N_3 - [\frac{1}{2}(N_1 + 1)])$ (that is 10 for $N_1 = 2, N_3 = 6$: in this case, the even streamwise mode subspace is the zero streamwise mode subspace). Here $[x]$ indicates the integer part of x.

The last invariance is that of the subspace $a_{-l,k} = a^*_{l,k}$ which, in the physical space, corresponds to structures invariant under reflection about a plane $x_3 = 0$. This can be easily seen by expanding the equations $u_i(x_3) = \epsilon_i u_i(-x_3)$ (where ϵ_i is equal to $+1$ if $i = 1$ or 2, -1 if $i = 3$) in terms of the expansion (2) and using the relations between $a_{l,-k}$ and $a_{l,k}$. The dimension of this subspace is $2(N_1 N_3 - 1)$ (that is 22 for $N_1 = 2$, $N_3 = 6$). Note that integrating the set of ODEs in this subspace is equivalent to imposing the cross-stream reflection symmetry of the flow *instantaneously*. Since we allow the flow structures to evolve asymmetrically, we deal with the complete $2((2N_1 - 1)N_3 - N_1)$ (that is 32 for $N_1 = 2$, $N_3 = 6$) dimensional dynamical system.

In the next section we present detailed results on integration of systems of equations with $N_1 = 2$ and $N_1 = 3$. We restrict the number of spanwise modes to 6. This leads to systems of dimension 32 (for $N_1 = 2$) and 54 (for $N_1 = 3$). One important consequence of the symmetries listed above is that some low-order models are invariant subspaces of higher-order ones. For example, as we have shown above, the $l = 0$ space is an invariant subspace. Consequently, if we start from a 32- or 54-dimensional system with zero values for all non-zero l values of $a_k^{(n)}$ then these coefficients will remain zero for ever and the solutions obtained are those of the 10D system (they are minor differences due to the Heisenberg model).

6. Results of numerical simulations

Numerical integrations have been carried out for models which include 1 and 2 non-zero streamwise modes and 1 or 2 modes in the normal directions, keeping 6 spanwise Fourier modes with a periodic box length $L_3^+ = 333$. A Runge–Kutta–Verner method of fifth- and sixth-order was used in double-precision arithmetic and these computations were carried out on an IBM 3090. The algorithms were checked by computations starting from initial conditions chosen to satisfy the various invariant subspaces discussed in §5.2.

6.1. *32-dimensional model*

We now outline the behaviour of typical solutions of systems including 1 normal mode and 2 streamwise Fourier modes with a periodic box length $L_1^+ = 666$ as the Heisenberg parameter α is reduced (we have not noticed the presence of various attractors in the phase space, other than those induced by the symmetry groups). When α is larger than 1.53, the trivial solution is the global attractor. For $1.51 \leqslant \alpha < 1.53$ we observe a non-zero fixed point in the ($l = 0$, even k) subspace. As α decreases from 1.50 to 1.22, the solution becomes intermittent in the zero streamwise mode subspace. This intermittency is similar to window I of intermittency present in the 10D model. In particular, bursts occur on a fast timescale

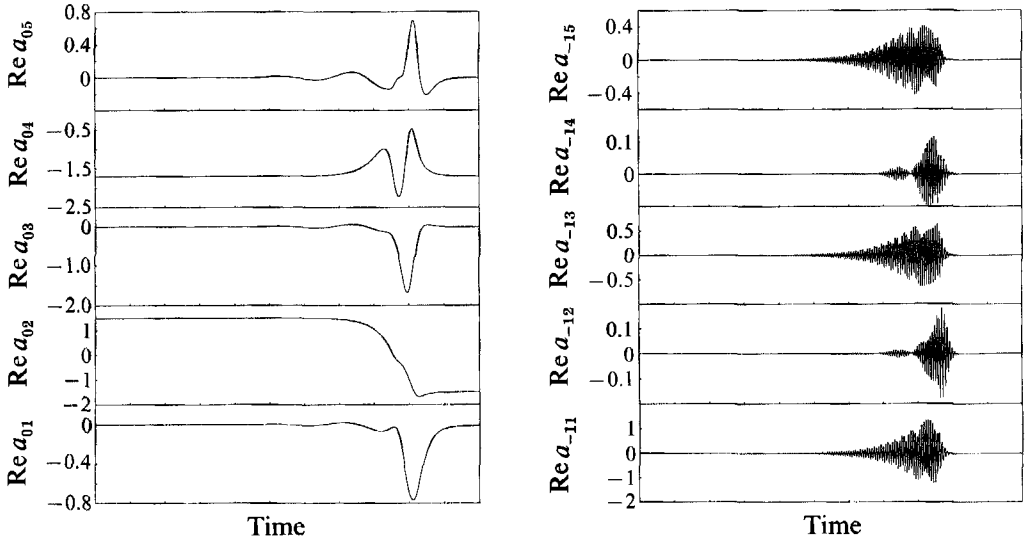

FIGURE 3. Typical solution in window III of intermittency from the 32D system. Time series of the real parts of $a_{01}, a_{02}, a_{03}, a_{04}, a_{05}, a_{-11}, a_{-12}, a_{-14}, a_{-15}$ for the parameter value $\alpha = 0.87$, for a time interval $\Delta t^+ = 5181$.

and do not involve any oscillatory motions. For $1.06 < \alpha \leqslant 1.22$, the solution, which is steady again, is a combination of the modes $a_{0,2}$ and $a_{0,4}$ only. Another window of intermittency, similar to that of window II of the 10D model, occurring in the zero streamwise mode subspace, appears for $0.91 \leqslant \alpha < 1.06$. The $a_{0,2}/a_{0,4}$ mixed modes destabilize in the $a_{0,1}/a_{0,3}/a_{0,5}$ directions. This solution encounters bursts involving growing oscillatory motions of the spanwise even and odd modes, corresponding to cross-stream oscillations of the streamwise rolls followed by a sudden breakup. So far, the sequence and nature of the solutions are very similar to those observed in the 10D model, indicating that the zero streamwise mode subspace is attracting. In these solutions, the non-zero streamwise modes are inactive after a very short transient during which they decay to zero. As α decreases further, the invariant zero streamwise subspace becomes unstable, namely streamwise instabilities occur. For $0.80 \leqslant \alpha < 0.91$, we observe a third window of intermittency. Between the bursts, the solution remains quasi-steady as in the first and second windows, staying in a neighbourhood of one equilibrium in the zero streamwise/even spanwise subspace. It then changes significantly during the bursts due to the participation of all modes to the dynamics. In the figures, we have normalized the a_k values with the square roots of the eigenvalues $\lambda_k^{\frac{1}{2}}$. Figure 3 reproduces time series for the real part of a few a_k values, and some selected projections of the phase space dynamics in figure 4 show evidence of a heteroclinic cycle connecting the two fixed points of the S^1-circle of solutions (corresponding to the burst of figure 3). For $0.50 \leqslant \alpha < 0.80$, the solution is attracted to the zero streamwise subspace where it becomes much more complex, apparently chaotic. The transient shows that the heteroclinic cycle starts travelling and becomes unstable. At this time, the non-zero streamwise modes collapse. For lower values of α, $0.1 \leqslant \alpha < 0.4$, the $(l = 0)$-subspace is unstable again and a fourth window of intermittency arises, the time series for which are shown in figure 5. In the intermittent behaviour previously described (first three intermittency windows), the solution between the bursts is always quasi-steady due to the proximity of a fixed point. The new solution is different in nature: it is very disorganized, apparently chaotic between the bursts in the zero streamwise subspace and the degree of

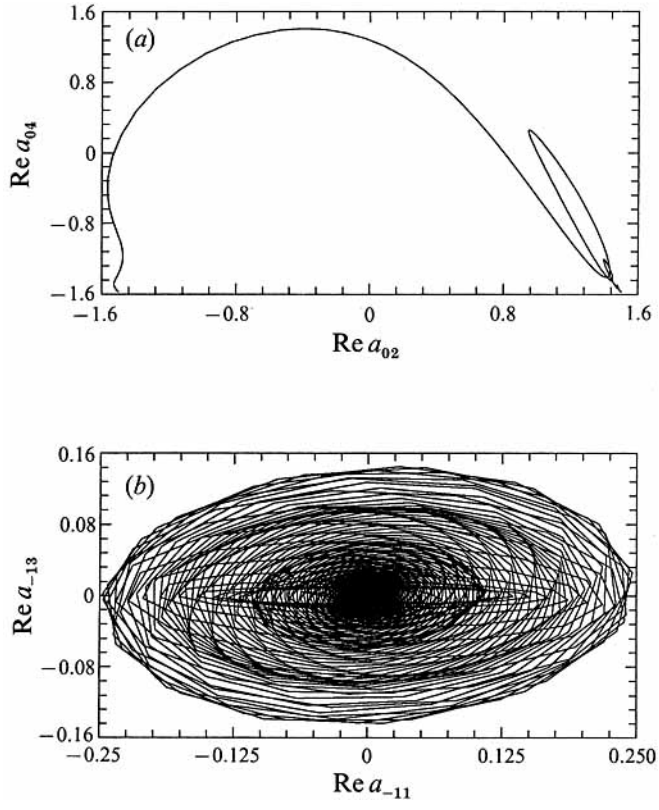

FIGURE 4. Selected projections of the phase space dynamics in window III of intermittency for the 32D system at the parameter value $\alpha = 0.87$, corresponding to the time series of figure 3. (*a*) Projection onto the $(\mathrm{Re}\,(a_{02}), \mathrm{Re}\,(a_{04}))$-plane showing one bursting event as the passage of the solution from one fixed point to the other. (*b*) Projection onto the $(\mathrm{Re}\,(a_{-11}), \mathrm{Re}\,(a_{-13}))$-plane showing one bursting event as a growing instability from, and the return to, the saddle fixed point.

complexity increases during each burst due to the sudden excitement of the non-zero streamwise modes of relatively high-frequency motions (compared with spanwise motions, see figures 3, 4*b*). As expected, in all the solutions involving non-zero streamwise modes, the frequencies are proportional to the wavenumber magnitude, a feature characteristic of travelling waves (as also found – see §3 – in the 10D model for low values of α although these waves propagate across the layer). This travelling solution propagates downstream at a convection velocity $u_c = 16$ (wall units), which is approximately equal to the mean velocity at the top of our layer ($y^+ = 40$). It is interesting to note that the downstream propagation speed is much faster than the spanwise oscillation speed, on the order of 0.4 (wall units). Travelling solutions are a consequence of the streamwise $SO(2)$ symmetry group invariance of the ODEs which is statistically satisfied by the solution itself (as in the real turbulent flow). From a physical viewpoint, it simply corresponds to the downstream advection of the structures by the mean flow (and is not, *a priori*, related to the existence of individual travelling waves such as those present in periodic solutions close to the instability onset, at low Reynolds number, as conjectured by Sirovich, Ball & Keefe 1990 and Zhou & Sirovich 1992). We speculate that the cause of the intermittency is the presence of an attracting heteroclinic cycle (in a generalized sense) which connects hyperbolic, apparently chaotic, limit sets. A projection of the phase space dynamics onto $(\mathrm{Re}\,(a_{-11}), \mathrm{Re}\,(a_{-13}))$ is similar to that of figure 4(*b*) in the third

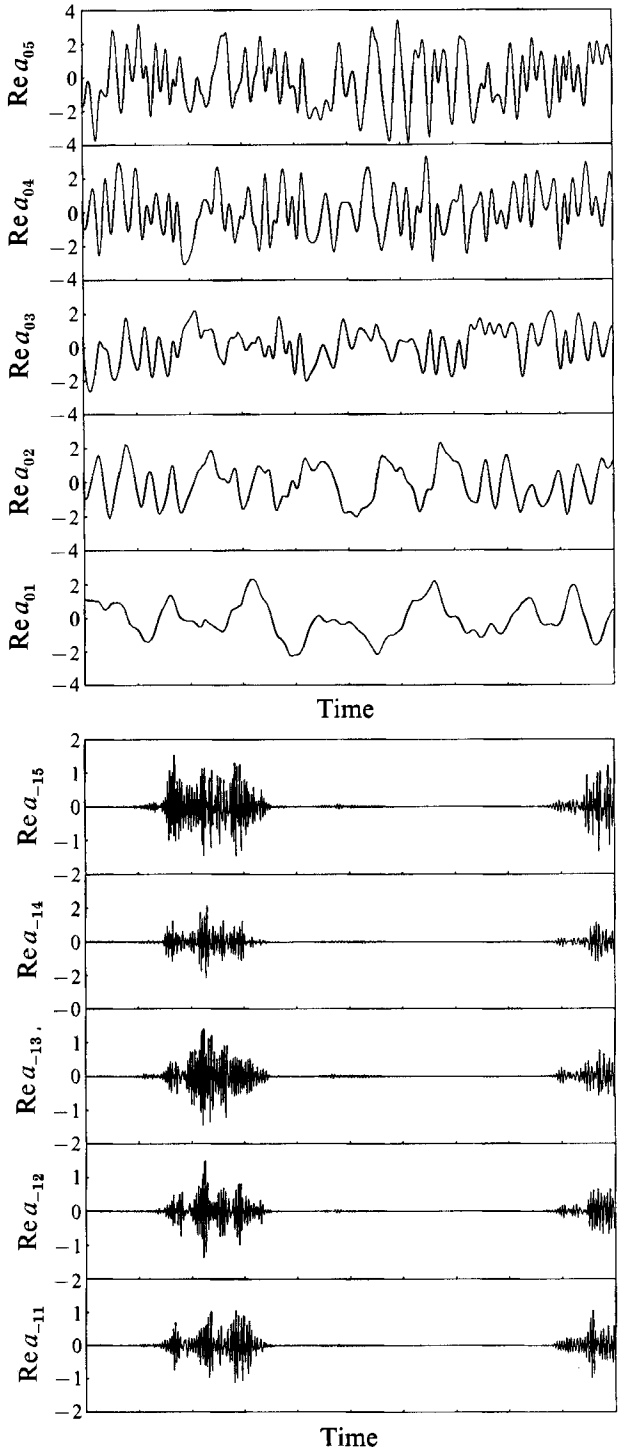

FIGURE 5. Typical solution in window IV of intermittency for the 32D system at the parameter value $\alpha = 0.2$, for a time interval $\Delta t^+ = 9420$. Time series of the real parts of a_{01}, a_{02}, a_{03}, $a_{04}, a_{05}, a_{-11}, a_{-12}, a_{-13}, a_{-14}, a_{-15}$ showing complex and intermittent dynamics in the zero and non-zero streamwise mode subspace, respectively.

Heisenberg parameter α	Behaviour
$\alpha \geqslant 1.53$	trivial solution: $a_{l,k} = \mathbf{0}$, $\forall(k,l)$ is the global attractor
$1.53 > \alpha \geqslant 1.51$	stable fixed point: $a_{02}, a_{04} \neq 0$, other modes are zero
$1.51 > \alpha \geqslant 1.22$	intermittency in the $a_{0,k}$ subspace: $a_{1,k} = \mathbf{0}$, $\forall k$ $a_{02}, a_{04} \neq \mathbf{0}$; $a_{0,k} = 0$, $\forall k \neq 2,4$ between bursts; $a_{0,k} \neq \mathbf{0}$, $\forall k$ during bursts (no oscillations)
$1.22 > \alpha \geqslant 1.06$	stable fixed point: $a_{02}, a_{04} \neq 0$, other modes are zero
$1.06 > \alpha \geqslant 0.91$	intermittency in the $a_{0,k}$ subspace: $a_{1,k} = \mathbf{0}$, $\forall k$; $a_{02}, a_{04} \neq \mathbf{0}$; $a_{0,k} = 0$, $\forall k \neq 2,4$ between bursts; $a_{0,k} \neq \mathbf{0}, \forall k$ during bursts (a_{01}, a_{03}, a_{05} oscillate)
$0.91 > \alpha \geqslant 0.8$	intermittency in the full space: $a_{02}, a_{04} \neq \mathbf{0}$; $a_{0,k} = 0$, $\forall k \neq 2,4$ between bursts; $a_{l,k} \neq \mathbf{0}$, $\forall l,k$ during bursts
$0.8 > \alpha \geqslant 0.5$	complex behaviour in the $a_{0,k}$ subspace: $a_{1,k} = \mathbf{0}$, $\forall k$; $a_{0,k} \neq \mathbf{0}$, $\forall k$
$0.4 > \alpha \geqslant 0.1$	intermittency in the full space: complex behaviour in the $a_{0,k}$ subspace between bursts; $a_{l,k} \neq \mathbf{0}$, $\forall(l,k)$ during bursts
$0.1 > \alpha$	complex behaviour in the full space: $a_{l,k} \neq \mathbf{0}$, $\forall(l,k)$

TABLE 1. Qualitative dynamical behaviour in the 32-dimensional system. **0** denotes the zero complex number.

intermittency window. The saddle, however, is no longer a fixed point but a complex orbit lying in the zero streamwise subspace and it resembles the complex solution obtained when the initial condition lies in the zero streamwise subspace. For an initial condition outside of any invariant subspace, the solution leaves the 10D zero streamwise subspace, starts a brief travelling excursion in the full 32D phase space and comes back to the zero streamwise subspace. The homoclinic connection of apparently chaotic sets by travelling orbits has also been observed in a spatio–temporal chaotic regime of the Kuramoto–Sivashinsky equation (Aubry & Lian 1992*a*). In table 1, we summarize the different solutions observed in this model.

Since the first three types of intermittency appear through bifurcations from fixed points, we investigate the nature of these bifurcations. This was done in Aubry *et al.* (1988) for the 10D dynamical system in which the second window of intermittency appeared through a subcritical Hopf bifurcation. As in their study, we can limit our stability calculation, without loss of generality, to one of the two real fixed points: $a_{02} = -r_2, a_{04} = -r_4$, where r_2 and r_4 are strictly positive values and all other components are zero. The results are identical for any pair of diametrically opposite fixed points of the symmetric S^1-circle. Linearization of the full system at this equilibrium involves the 32×32 matrix block which diagonalizes as follows: $(\mathrm{Re}\,(a_{02}), \mathrm{Re}\,(a_{04}))$, a 2×2 matrix; $(\mathrm{Im}\,(a_{02}), \mathrm{Im}\,(a_{04}))$, a 2×2 matrix; $\mathrm{Re}\,(a_{01})$, $\mathrm{Re}\,(a_{03}), \mathrm{Re}\,(a_{05}))$, a 3×3 matrix; $(\mathrm{Im}\,(a_{01}), \mathrm{Im}\,(a_{03}), \mathrm{Im}\,(a_{05}))$, a 3×3 matrix; $(a_{-11}, a_{-13}, a_{-15}, a_{11}, a_{13}, a_{15})$, a 12×12 matrix; and $(a_{-12}, a_{-14}, a_{10}, a_{14})$, a 10×10 matrix. Selected eigenvalues (specifically those showing bifurcations) of these matrices are presented in Appendix B.† One eigenvalue of $(\mathrm{Im}\,(a_{02}), \mathrm{Im}\,(a_{04}))$ has zero real part which corresponds to variations along the S^1-circle of fixed points, its eigenvector being tangent to this circle. The eigenvalues of the matrices involving non-zero streamwise wavenumbers are always complex conjugate numbers due to the travelling character of the solution. For parameter values greater than 1.50, all eigenvalues have negative real parts, showing that the fixed point is stable. The first bifurcation occurs at $\alpha = 1.51$ at which an eigenvalue becomes positive in the imaginary part of zero streamwise, odd spanwise mode subspace. The fixed point becomes a saddle with a one-dimensional unstable manifold. This corresponds to the

† Full tables of the eigenvalues can be obtained from the authors or the Editorial Office.

Heisenberg parameter α	Behaviour
$\alpha \geqslant 2.1$	trivial solution: $a_{l,k} = \mathbf{0}$, $\forall (l,k)$ is the global attractor
$2.1 > \alpha \geqslant 2.05$	stable fixed point: $a_{02}, a_{04} \neq 0$, other modes are zero
$2.05 > \alpha \geqslant 1.84$	intermittency (I) in the $a_{0,k}$ subspace: $a_{1,k} = \mathbf{0}$, $\forall k$; $a_{02}, a_{04} \neq \mathbf{0}$; $a_{0,k} = 0$, $\forall k \neq 2, 4$ between bursts; $a_{0,k} \neq \mathbf{0}$, $\forall k$ during bursts (no oscillations)
$1.84 > \alpha \geqslant 1.43$	stable fixed point: $a_{02}, a_{04} \neq 0$, other modes are zero
$1.43 > \alpha \geqslant 1.23$	intermittency (II) in the $a_{0,k}$ subspace: $a_{1,k} = \mathbf{0}$, $\forall k$; $a_{02}, a_{04} \neq \mathbf{0}$; $a_{0,k} = \mathbf{0}$, $\forall k \neq 2, 4$ between bursts; $a_{0,k} \neq \mathbf{0}$, $\forall k$ during bursts (a_{01}, a_{03}, a_{05} oscillate)
$1.23 > \alpha \geqslant 1.18$	intermittency (III) in the full space: $a_{02}, a_{04} \neq \mathbf{0}$; $a_{0,k} = 0$, $\forall k \neq 2, 4$ between bursts; $a_{l,k} \neq \mathbf{0}$, $\forall l, k$ during bursts
$1.18 > \alpha \geqslant 0.6$	complex behaviour in the $a_{0,k}$ subspace: $a_{1,k} = \mathbf{0}$, $\forall k$; $a_{0,k} \neq \mathbf{0}$, $\forall k$
$0.6 > \alpha \geqslant 0.4$	intermittency (IV) in the full space: complex behaviour in the $a_{0,k}$ subspace between bursts; $a_{l,k} \neq \mathbf{0}$, $\forall l, k$ during bursts
$0.4 > \alpha$	complex behaviour in the full space: $a_{l,k} \neq \mathbf{0}$, $\forall l, k$

TABLE 2. Qualitative dynamical behaviour in the 54-dimensional system. **0** denotes the zero number.

appearance of the first window of intermittency. The fixed point recovers its stability in a small window (all eigenvalues are negative for $\alpha = 1.10$ and 1.20) and a Hopf bifurcation occurs at $\alpha = 1.06$, consistently with numerical integrations which show that solutions become intermittent again. The fixed point is then a saddle with a two-dimensional unstable manifold in the zero streamwise, odd spanwise subspace. Another Hopf bifurcation occurs at about $\alpha = 0.91$, where an eigenvalue crosses the imaginary axis in the non-zero streamwise, odd spanwise subspace. This opens the third window of intermittency where the non-zero streamwise modes burst along with the zero streamwise, odd spanwise modes. The fixed point becomes a saddle point with a four-dimensional unstable manifold. At the other real fixed point, $a_{02} = +r_2, a_{04} = -r_4$, the eigenvalues are all the same, except those of the real and imaginary part of (a_{01}, a_{03}, a_{05}) which are interchanged, making the unstable manifolds in the first and second windows of intermittency lie in the $(\mathrm{Re}\,(a_{01}), \mathrm{Re}\,(a_{03}), \mathrm{Re}\,(a_{05}))$, instead of $(\mathrm{Im}\,(a_{01}), \mathrm{Im}\,(a_{03}), \mathrm{Im}\,(a_{05}))$ subspace. At all other points of the circle, the unstable manifold is a rotation of one of these two manifolds and all odd spanwise modes burst, as seen in numerical integrations of the system.

In this stability analysis, we have shown that the first two windows of intermittency appear from a linear instability of the equilibria in the zero streamwise subspace while the third window emerges through a linear instability of the non-zero streamwise modes. In all cases, the unstable manifold of the fixed points lies in the odd spanwise subspace. Nevertheless, the numerical integration shows that the non-zero streamwise, even spanwise modes burst as well, which can be understood through the nonlinear action of the quadratic terms $a_{l'k'} a_{l-l',k-k'}$. Obviously, if k is even, k' and $k-k'$ are both odd or even and if k is odd, one is odd and the other even. This implies that if odd spanwise modes burst, the even spanwise modes get triggered by quadratic nonlinearities involving odd/odd spanwise mode interactions. Moreover, once the even spanwise modes are carried sufficiently far away from the fixed-point values, the nonlinear even/even spanwise modes interactions also contribute to the burst. This leads to a nonlinear instability which is delayed in time as observed in time series (figure 3).

The results have been obtained using a computational cell of 666 wall units in the

x_1 direction. Carrying out integrations using cells of streamwise lengths 1000 and 2000 wall units, we observe the same heteroclinic connections.

6.2. *54-dimensional model*

We now investigate the action of a second streamwise harmonic on the previous system which leads to 54 dimensions keeping the streamwise length of the box $L_1^+ = 666$. Both the properties and the solutions of the equations are similar to those of the 32D model. The numerical integration of the equations leads to the bifurcation behaviour shown in table 2 and time series of typical solutions in window III are displayed in figure 6.

As in the case of the 32D dynamical system, we compute the eigenvalues of the Jacobian matrix at the fixed point $a_{02} = -r_2, a_{04} = -r_4$. Linearization of the full system is achieved by studying the 54×54 matrix block which diagonalizes as follows: $(\mathrm{Re}\,(a_{02}), \mathrm{Re}\,(a_{04}))$, a 2×2 matrix; $(\mathrm{Im}\,(a_{02}), \mathrm{Im}\,(a_{02}))$, a 2×2 matrix; $(\mathrm{Re}\,(a_{01}), \mathrm{Re}\,(a_{03}), \mathrm{Re}\,(a_{05}))$, a 3×3 matrix; $(\mathrm{Im}\,(a_{01}), \mathrm{Im}\,(a_{03}), \mathrm{Im}\,(a_{05}))$, a 3×3 matrix; $(a_{-12}, a_{-14}, a_{10}, a_{12}, a_{14})$, a 10×10 matrix; $(a_{-11}, a_{-13}, a_{-15}, a_{11}, a_{13}, a_{15})$, a 12×12 matrix; $(a_{-21}, a_{-23}, a_{-25}, a_{21}, a_{23}, a_{25})$, a 12×12 matrix; and $(a_{-22}, a_{-24}, a_{20}, a_{22}, a_{24})$, a 10×10 matrix. Selected eigenvalues (specifically those showing bifurcations) of these matrices are presented in Appendix C.† As in the 32D dynamical system, we observe the first two bifurcations through which the first and second windows of intermittency appear in the $(\mathrm{Im}\,(a_{01}), \mathrm{Im}\,(a_{03}), \mathrm{Im}\,(a_{05}))$ subspace. The third window emerges through a (subcritical) Hopf bifurcation occurring in the $(a_{-11}, a_{-13}, a_{-15}, a_{11}, a_{13}, a_{15})$ subspace. Although the eigenvalues of the second non-zero streamwise mode subspace stay negative for all these parameter values, numerical integrations show that the second non-zero streamwise modes burst as well as the first one. As for the excitation of even spanwise modes in the 32D model, the second streamwise modes become activated, with a delay, through nonlinear quadratic interactions. Odd spanwise modes become destabilized first, followed by the even spanwise modes (for the reason mentioned above).

In view of the hierarchy of instabilities presented above, one can ask whether higher-order streamwise harmonics will burst as well. Experimental visualizations have shown that sublayer bursting events are characterized by generation of fine-scale turbulence. It is obvious that this cascade of energy towards finer scales is not limited to two harmonics. The study of the 54D dynamical system shows that once the first non-zero streamwise modes burst through a subcritical Hopf bifurcation, the second non-zero streamwise modes burst also due to nonlinear interactions. Would higher harmonics be triggered in the same manner? This is obviously the case as an examination of the quadratic terms reveals: in the same way the $l = 2$ modes are destabilized due to $l = 1/l = 1$ interactions, the $l = 3$ modes due to $l = 1/l = 2$ interactions, the $l = 4$ modes due to $l = 1/l = 3$ and $l = 2/l = 2$ interactions, etc.

6.3. *Models involving two normal modes*

We now briefly describe results obtained from a model involving two normal modes, two streamwise Fourier modes and six spanwise Fourier modes, including 64 dimensions, the periodic box size being the same as in the two previous sections. At large α values, we observe the stable trivial (zero) solution from which a fixed point in the $a_{0,2}^{(n)}, a_{0,4}^{(n)}$ $(n = 1, 2)$ space bifurcates. As α is reduced further, a fixed point in the $a_{0,k}^{(n)}$ $(n = 1, 2;\ k = 1, \ldots 5)$ subspace becomes stable. For lower α values, a window of intermittency appears, where the non-zero streamwise modes become excited intermittently. Solutions stay quasi-steady in the zero streamwise subspace before

† Full tables of the eigenvalues can be obtained from the authors or the Editorial Office.

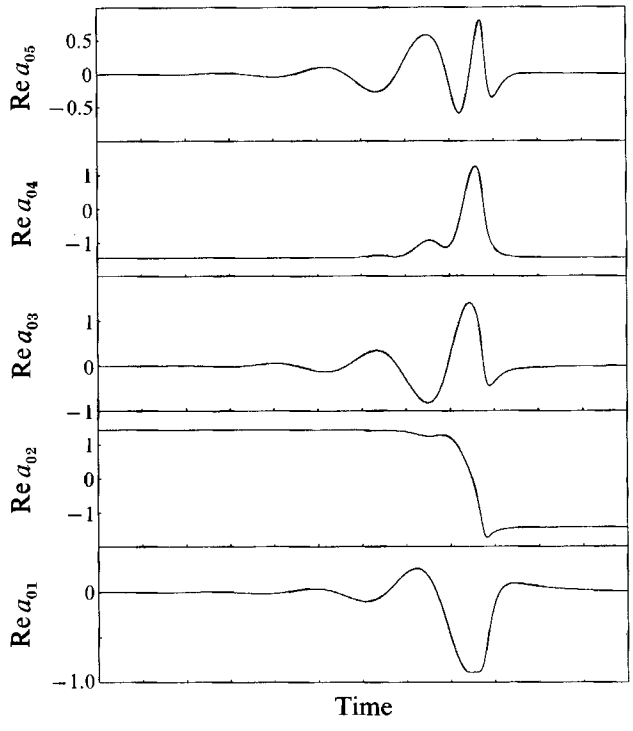

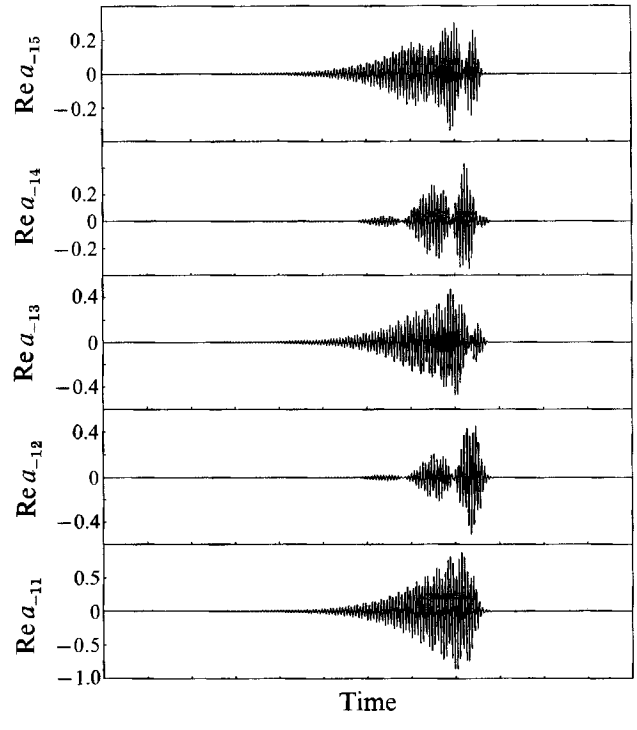

FIGURE 6. For caption see facing page.

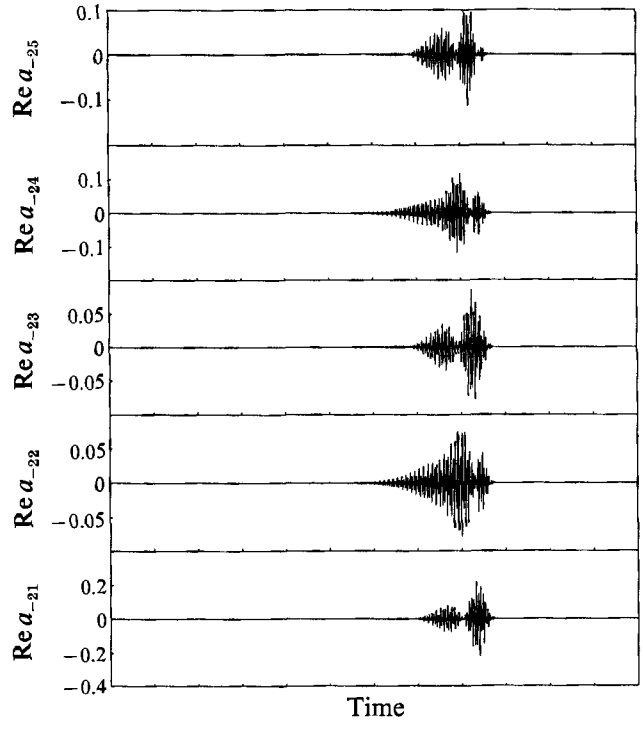

FIGURE 6. Typical solution in window III of intermittency for the 54D system at the parameter value $\alpha = 1.2$, for a time interval $\Delta t^+ = 5652$. Time series of the real parts of $a_{01}, a_{02}, a_{03}, a_{04}, a_{05}, a_{-11}, a_{-12}, a_{-13}, a_{-14}, a_{-15}, a_{-21}, a_{-22}, a_{-23}, a_{-24}, a_{-25}$.

Heisenberg parameter α	Behaviour
$\alpha \geqslant 1.9$	trivial solution: $a_k^{(n)} = \mathbf{0}$, $\forall(n,l,k)$ is the global attractor
$1.9 > \alpha \geqslant 1.7$	stable fixed point $a_{0,2}^{(n)}, a_{0,4}^{(n)} \neq 0$, $\forall n$, other modes are zero
$1.7 > \alpha \geqslant 0.9$	stable fixed point: $a_{0,k}^{(n)} \neq \mathbf{0}, \forall(n,k)$, other modes are zero
$0.9 > \alpha \geqslant 0.6$	intermittency in the full subspace $a_{0,k}^{(n)} \neq \mathbf{0}, \forall(n,k)$ between bursts; $a_{l,k}^{(n)} \neq \mathbf{0}, \forall(n,l,k)$ during bursts
$0.6 > \alpha \geqslant 0.4$	complex solution: $a_{l,k}^{(n)} \neq \mathbf{0}, \forall(n,l,k)$
$0.4 > \alpha \geqslant 0.2$	intermittency in the full space similar to window IV in the 32D model: complex behaviour in the $a_{0,k}^{(n)}$ subspace $\forall(n,k)$ between bursts; $a_{l,k}^{(n)} \neq \mathbf{0}, \forall(n,l,k)$ during bursts
$0.2 > \alpha$	complex solution: $a_{l,k}^{(n)} \neq \mathbf{0}, \forall(n,l,k)$

TABLE 3. Qualitative dynamical behaviour in the 64-dimensional system. **0** denotes the zero complex number.

and after bursting. As α is reduced further, we observe a solution similar to the fourth window of intermittency in the systems discussed above. The details of the bifurcation behaviour are given in table 3.

7. Identification of flow structures

We now concentrate on the kinematics and dynamics of 'coherent structures' as they appear in our models. Structures of different types have been extensively investigated from both visualization experiments and direct numerical simulations.

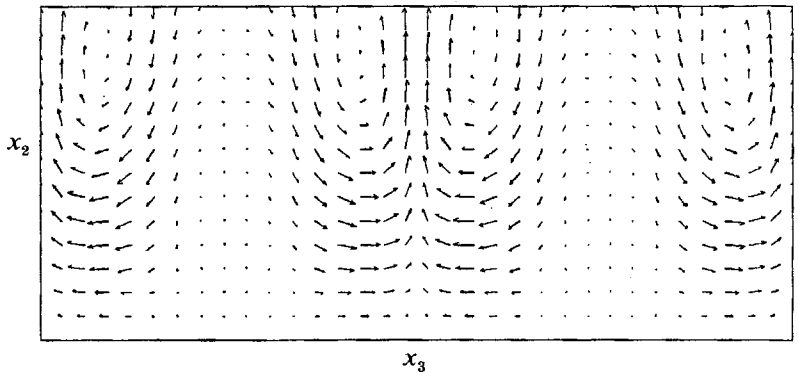

FIGURE 7. Vector representation of a cross-section of the flow, i.e. the two velocity components u_2, u_3 in an (x_2, x_3)-plane during a 'quiescent' period of the intermittent solution at the parameter value $\alpha = 0.87$. The spanwise (horizontal) and normal (vertical) dimensions of the box are 333 and 40 wall units respectively.

However, the connection between these structures is not yet well understood. We show that most structures previously reported in the literature are present in our systems and that they are all connected to each other. To illustrate this connection, we first describe the fixed-point solutions in physical space. We then analyse flow fields during bursts, concentrating on both the spatial distribution of flow patterns and their temporal behaviour. The solutions discussed in this and the next sections have been obtained via integrations of the 32-dimensional system discussed in §6.1. Clearly, solutions of higher-dimensional models previously studied lead to similar results.

7.1. *Structures in a fixed-point solution*

Every fixed point, or steady solution, described above appears in the $(k_1 = 0)$-subspace, representing infinitely long structures in the streamwise direction. Although such a flow arises as an artifact of the unrealistically large value of the transport coefficient α, it gives insight into the physics of more complicated solutions. This is because the rolls it represents are a recurrent basic pattern contained in realistic flows, themselves being connected to other types of structures. To illustrate this, we follow Kline & Robinson's (1990) survey where one can find a complete description of a rich variety of structures identified in a large number of contributions (see also Robinson's 1991 review). We now discuss only the first five structure categories as the others seem to have been observed by a few researchers only or are not relevant to the present work (outer structures, for instance). Figure 7 (see also the fixed-point solution in Aubry *et al.* 1988) shows a vectorial plot of the instantaneous velocity components u_2 and u_3 in a cell of dimension 40×333 lying in the (x_2, x_3)-plane. The flow field consists of counter-rotating roll pairs with the updraft regions in between the rolls located at $x_3 = 0$ and $x_3 = 167$. In this simplistic solution, the rolls are symmetric and always occur in pairs. This is merely a consequence of the reflection symmetry of the two-point correlations (and the equations) which is then satisfied by the solution itself *instantaneously*.

7.1.1. *Low speed streaks in the region $x_2 < 10$*

Streaks or streamwise filaments of low-speed outward-moving fluid observed in the near-wall region, have been observed by Kline *et al.* (1967). Since then, their

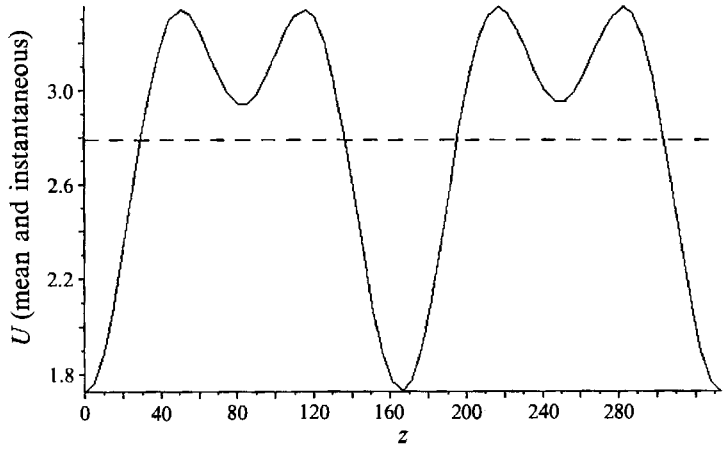

FIGURE 8. Distribution of the streamwise velocity component, mean (U) (– – – –) and instantaneous ($U+u$) (——), as a function of x_3^+ at $x_2^+ = 2.8$ from the intermittent solution at the parameter value $\alpha = 0.87$ in the 32D system.

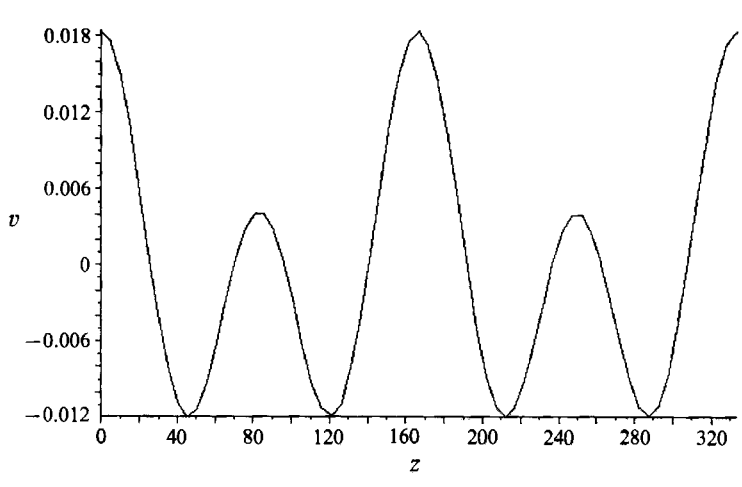

FIGURE 9. Distribution of the normal velocity component u_2 as a function of x_3^+ at $x_2^+ = 2.8$ from the intermittent solution at the parameter value $\alpha = 0.87$ in the 32D system.

existence has been reported by many researchers in the field who all agree on a mean spanwise spacing of approximately 100 wall units. Smith & Metzler (1983) found that the probability distribution function of the low-speed structure around the mean value of 100 wall units is log-normal and has a dense range from 60 to 180 wall units.

We now seek the location of the slow outward-moving streaks from our results. Figure 8 represents the mean and instantaneous streamwise velocity profiles, U and $\tilde{u}$, as a function of spanwise location at the wall distance $x_2 = 2.8$ while figure 9 shows the normal component, v. It is clear that the slow fluid located at $x_3 = 0$ and $x_3 = 166$, in between the rolls (see figure 7) has maximum, positive normal velocity and corresponds to the outward-moving streaks (consistently with other authors' findings (e.g. Blackwelder & Eckelmann 1979)). The spanwise extent of such streaks is about 30 viscous lengths, in agreement with experimental observations.

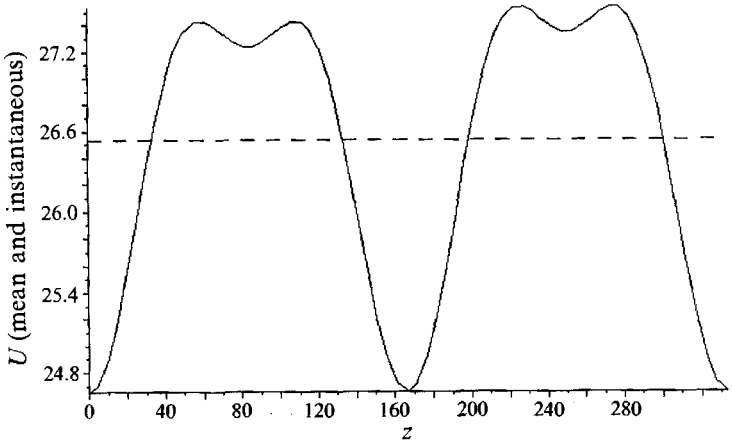

FIGURE 10. Distribution of the streamwise velocity, mean (U) (– – – –) and instantaneous ($U+u$) (——), as a function of x_3^+ at $x_2^+ = 38.5$ from the intermittent solution at the parameter value $\alpha = 0.87$ in the 32D system.

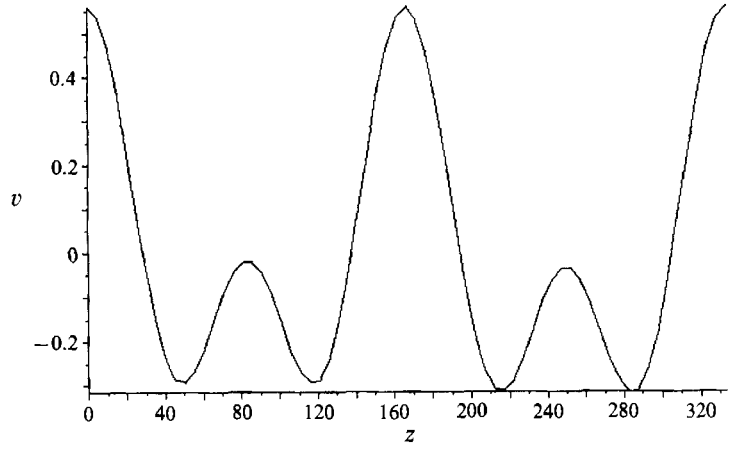

FIGURE 11. Distribution of normal velocity u_2 as a function of x_3^+ at $x_2^+ = 38.5$ from the intermittent solution at the parameter value $\alpha = 0.87$ in the 32D system.

7.1.2. *Ejections*

The low-speed streaks in the sublayer get slightly lifted away from the wall as they propagate downstream until they reach a location at which their rate of ejection increases significantly. These ejection motions, which have been termed lifting (e.g. Kim *et al.* 1971; Corino & Brodkey 1969; Willmarth & Lu 1972, Smith & Metzler 1983; and other workers), are experimentally observed primarily in the region $10 < x_2 < 40$.

Ejections are clear in figure 7 where strong outward motions are located in between the rolls, above the sublayer streaks. (See also figures 10 and 11 where the streamwise and normal velocity components are presented as a function of x_3, at $x_2 = 38.5$.) In this flow picture, the normal velocity increase is simply due to the conservation of mass. This suggests that streaks and ejections are a part of the same structure, without the need for any dynamics to be involved. However, ejections can be weakened or strengthened by lateral motions of the rolls with respect to each other.

7.1.3. *Sweeps of high-speed fluid towards the wall*

While flow visualizations do not clearly exhibit inward sweeps of high-speed fluids, their presence is needed from continuity and has been detected by quadrant analysis (Willmarth & Lu 1972; Willmarth & Bogar 1977). They have been shown to significantly contribute to the Reynolds shear stress, and therefore to the turbulence production.

It is clear from figures 7, 8 and 9 that the spanwise outer regions of the rolls where fluid moves toward the wall have an excess streamwise velocity compared to the mean, thus constituting the sweeps. Also, in agreement with experimental findings, the sweep regions observed here are larger compared with the streaks.

To conclude, the picture of the rolls, in the framework of sweeps and streaks, can be described as alternate regions of elongated patterns of fluid having high and low streamwise momentum (see e.g. Gupta, Laufer & Kaplan 1971).

7.1.4. *Vortical structures*

Let us first recall that there has been some controversy concerning the definition of three-dimensional vortical structures. Robinson *et al.* (1990) propose identifying near-circular fluid paths, around a core, in the frame of reference of the core. Other researchers plot contours of constant enstrophy or trace vortex lines in three-dimensional space. In this paper we adopt the last possibility. Vortical structures identified so far in the wall region fall essentially in two broad categories. The first of these consists of horseshoe or hairpin shaped structures, the existence of which was first proposed by Theodorsen (1952). Later, using a smoke visualization technique, Head & Bandyopadhyay (1981) established the presence of elongated hairpin vortices at high Reynolds number and less elongated horseshoe vortices at low Reynolds numbers. Moin & Kim (1982) obtained evidence for the existence of such structures in a direct numerical simulation of a channel flow, while Kim (1987) studied their temporal evolution. The second vortical structure category detected in wall turbulence is that of 'streamwise vortices', corresponding to nearly circular patterns in the streamlines of the fluctuating flow cross-section. Bakewell & Lumley (1967) and Blackwelder & Eckelmann (1979) used statistical techniques to establish their existence (actually the first authors used the POD), Smith & Schwartz (1983), investigating individual realizations, show that vortices are present at a given point only intermittently.

Clearly, the rolls in figure 7 correspond to what other authors refer to as 'streamwise vortices', although the vorticity is not only streamwise. In fact, we now show that the vortex lines corresponding to a pair of counter-rotating rolls have a horseshoe shape. Noting that the spanwise gradient of the streamwise velocity is negative in the left roll and positive in the right one and recalling that streamwise variations are small, it is easy to see that the normal vorticity is negative in the left roll and positive in the right one. Moreover, the spanwise vorticity, which essentially originates from the mean velocity gradient, is negative in both regions. This elementary argument implies that the vortex lines have a horseshoe shape with its head lying in between the rolls. If the circulation plane of the rolls is inclined to the wall (which is indeed the case so that the Reynolds shear stress is non-zero), the vortex lines are also inclined. Vortex lines with a horseshoe shape are shown in figure 12. Consistently with this scenario, a larger mean velocity, characteristic of higher Reynolds numbers, would increase the Reynolds shear stress by decreasing the mean distance between two rolls of the same pair and would make horseshoes more narrow

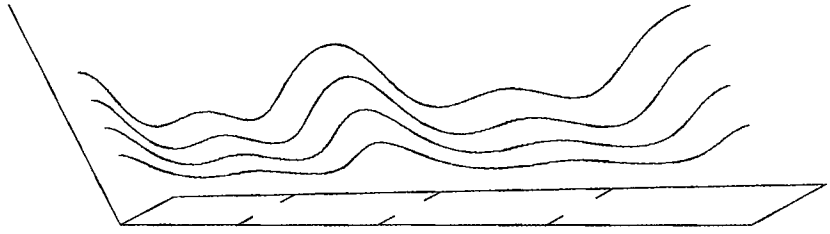

FIGURE 12. Vortex lines at various vertical (x_2) positions during a 'quiescent' period of the solution at the parameter value $\alpha = 0.87$ in the 32D system. The horizontal plane is (x_1, x_3), x_1 being the largest dimension.

and more elongated. Following the above arguments, it is clear that the reflection symmetry of the rolls accounts for the symmetry of the horseshoe. In more complex solutions, and most probably in the real flow, both the rolls and the horseshoe will be asymmetrical most of the time. In particular, when a roll is isolated, the vortex lines take a 'hook-like' shape.

7.1.5. *Near-wall shear layers*

Shear layers with a normal and spanwise gradient of streamwise velocity have been identified, for example by Corino & Brodkey (1969) visualizing the flow, and by Kreplin & Eckelmann (1979) and by Johansson, Alfredsson & Eckelmann (1987) using probe measurements. Changes in the streamwise velocity have also been detected by VITA techniques (see e.g. Bogard & Tiederman 1987). Recently, Jimenez *et al.* (1988) used contours of spanwise vorticity in a numerically simulated channel flow to establish that the near-wall region is dominated by intense three-dimensional shear layers, whose instability should lead to bursts. Blackwelder & Swearingen (1990) compared streamwise vortices near a flat wall with Görtler vortices next to a concave wall. They argue that, in both cases, these vortices are the cause of inflexion points in the $U(z)$ profile.

The presence of rolls in our model leads to both vertical and horizontal shear layers. While the former comes from the juxtaposition of slow and fast fluid (streaks and sweeps) in the spanwise direction (see figures 7 and 8), the latter is a feature of the streamwise velocity gradient: an inflexion point arises in the sweep region at the interface between the fluid very close to the wall which is accelerated in its sweep motion and that slightly away ($x_2 > 15$).

7.1.6. *Concluding remarks on the structures*

We find a one-to-one correspondence between the various patterns previously reported in the near-wall turbulence literature. Streamwise rolls, streaks, sweeps, horseshoe shaped vortical structures and shear layers are all a part of the same structure: all depends on which physical quantity is investigated. It is particularly interesting to note that the horseshoe and rolls are merely the same entity (so that the rolls are not, strictly speaking, the legs of the horseshoe, as proposed by other authors). This relation suggests a simplistic mechanism for the rolls formation consisting in stretching of the spanwise vorticity of the laminar flow. Although we made the above observations based on a simplified solution, it is clear that these relations should remain valid *locally* in the real flow (as noticed above, the presence of a symmetric pair is only an artifact of both the steadiness of the solution and the spanwise reflection symmetry). Finally, we would like to point out that our

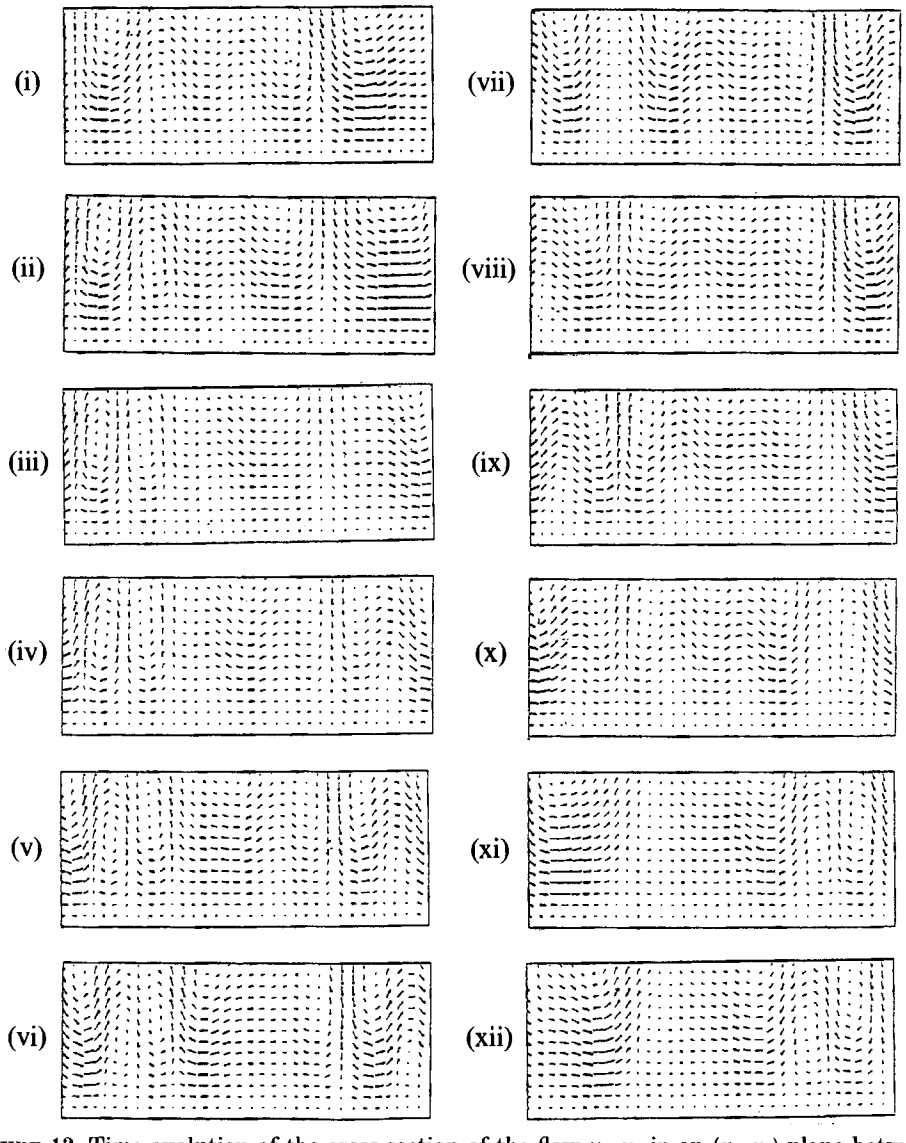

FIGURE 13. Time evolution of the cross-section of the flow u_2, u_3 in an (x_2, x_3)-plane between two bursts in window IV of intermittency for the 32D system at the parameter value $\alpha = 0.2$. The box dimensions are the same as those in figure 7. Time increases from (i) to (xii) with a time step of 37.68.

deductions are of a kinematical nature. Clearly, the rolls – and all the 'structures' associated with them – are dynamically active: they interact, move, break and re-form. In our fixed-point solution, these dynamics are damped by an excessive eddy viscosity introduced in the system. In the next paragraph, we describe the temporal behaviour of the eddies as we drop the artifical damping.

7.2. *Structures in time-evolving solutions*

So far we have described the eddy structure according to the steady solution of our models. When the flow gains some dynamics, as of course it does in real turbulence, observation of the temporal evolution of velocity vectors in a cross-section of the flow

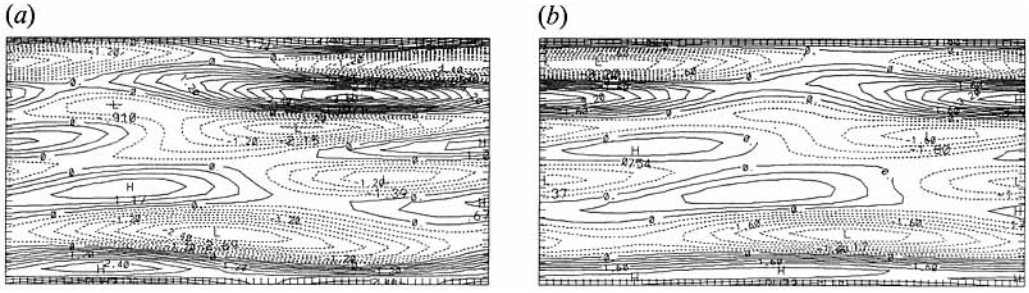

FIGURE 14. Contours of the streamwise velocity component u_1 in an (x_1, x_3) plane located at $x_2^+ = 5.6$, for a solution in window IV of intermittency when all the modes are activated in the solution shown in figure 13. Solid and dashed lines represent positive and negative values, respectively. Parts (*a*) and (*b*) correspond to two times such that $\Delta t^+ = 9.42$, showing the streak and sweep advection downstream at a speed $u_c \approx 16$. The streamwise (horizontal) and spanwise (vertical) dimensions of the box are 666 and 333 wall units respectively.

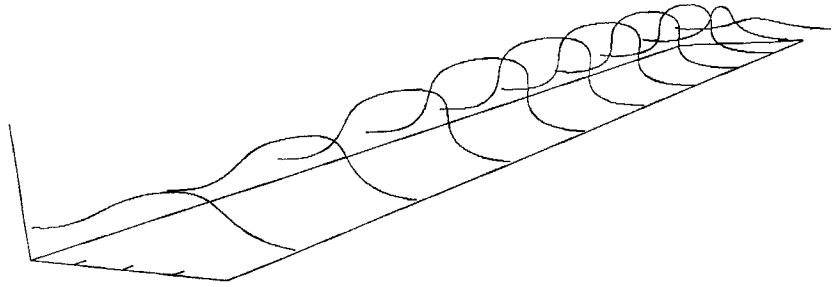

FIGURE 15. Instantaneous vortex lines at various streamwise locations during window IV of intermittency during a burst, i.e. when all the modes are excited in the solution shown in figure 13. The vertical axis is the normal direction and the mean flow is from lower left to upper right. The streamwise, spanwise and normal dimensions of the box are 450, 100 and 40 wall units respectively.

shows that the reflection symmetry is often broken (except in the first three windows of intermittency). Then 'structures' are very similar to those previously described, the main difference being that the rolls appear isolated or in asymmetric pairs. Figure 13 displays, for a parameter value $\alpha = 0.2$ (window IV of intermittency), instantaneous velocity vectors in the cross-stream plane during a time interval in between two bursts. Symmetric, asymmetric and isolated rolls are present, accompanied by sweeps, streaks, horseshoe (or hook-like) vortex lines and three-dimensional shear layers.

Since the relatively 'quiescent' periods between the bursts take place in the zero streamwise subspace, all physical structures are infinitely long in the streamwise direction during these times. However, as time evolves and the fluid particles are advected downstream, a streamwise instability takes place: this infinite dimension breaks up; the solution bursts into eddies of finite length which are advected downstream. Contours of the streamwise velocity fluctuations in an (x_1, x_3)-plane near the wall ($x_2 = 2.8$) are shown in figure 14. As expected, the patterns consist of elongated structures, streaks and sweeps. They have a streamwise length of about 500 wall units and a spanwise width of nearly 40 wall units. This figure resembles those obtained by other researchers (e.g. Moin & Kim 1982). The streamwise velocity contours for two different times (figure 14*a*, *b*) show the advection of the structures downstream at a speed $u_c \approx 16$, in agreement with our previous observation of the time series in §6. Figure 15 shows a perspective view of various vortex lines

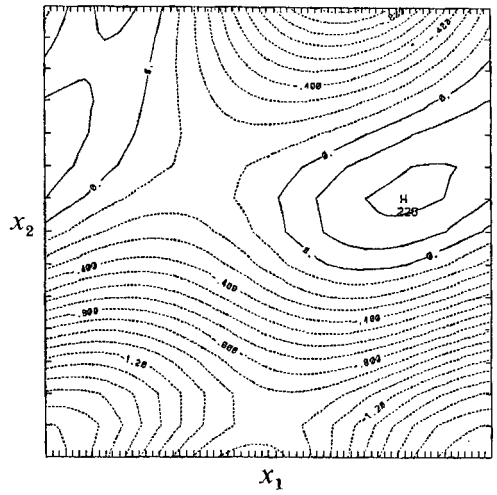

FIGURE 16. Contours of the spanwise vorticity in an (x_1, x_2)-plane located at $x_3^+ = 250$, for a solution in the window IV of intermittency in the 32D system at $\alpha = 0.2$ during a burst, i.e. when all the modes are activated. The streamwise and normal dimensions of the box are 666 and 40 respectively.

corresponding to a slow-moving streak in between two symmetric rolls: as explained in §7.1.4, these lines have a horseshoe shape. Our picture resembles that of Kim & Moin (1986) and Kim (1987). Figure 16 displays contours of spanwise vorticity in an (x_1, x_2)-plane in our solution and shows thin layers of spanwise vorticity protruding out from the wall as described by Jimenez *et al.* (1988) (up to $y^+ = 40$).

Finally, the bursting period is large, around 4000 time units at the parameter value $\alpha = 0.2$ for instance. As recalled above, the interburst time depends on both the eigenvalue with the largest positive real part λ_u and the 'external noise' present in the system. More precisely, one can write $T_b = (1/\lambda_u)(\ln(1/\epsilon) + O(1))$ where ϵ is the root mean square of the noise (see Stone & Holmes 1989, 1990). Our linear stability analysis of the 32D system gives a value for λ_u of about 0.2–0.4 in window II of intermittency while it is much higher in window III, around 1 at $\alpha = 0.87$ and even higher at lower α values. In the presence of numerical round-off errors only, it was observed in the 10D model that the interburst time increases with time. This effect, which should be present in an ideal system without noise, cannot be detected in the 32D (or 54D) model of this paper when streamwise modes become activated due to a much larger eigenvalue λ_u which prevents T_b from increasing even in the presence of reduced noise. Moreover, since the λ_u increases as α decreases, the interburst time, at the same noise level, decreases. For a most unstable eigenvalue on the order of 1, it is clear that the interburst timescaling depends on ϵ in an essential way. Pressure fluctuations at the top of the layer, neglected in the calculations presented here, may then play an important role in this scaling.

8. Criteria for the choice of a realistic Heisenberg parameter value

In this study, as in that of Aubry *et al.* (1988), we have used the Heisenberg parameter α as a bifurcation parameter. Although α should vary slightly in time, it has been assumed constant, as in Smagorinsky's model. The issue is then to determine realistic values of α. For instance, it is clear that solutions in the fourth window of intermittency represent more realistic velocity fields than the steady

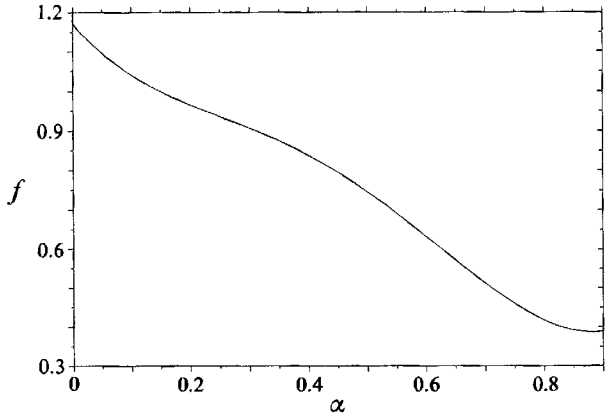

FIGURE 17. Distribution of the energy ratio f (see §8) as a function of the parameter α in the 32D system.

solutions obtained for large dissipation values. We now propose two criteria for selecting appropriate α values.

The first one consists in examining the kinetic energy content of the solutions obtained at various α values. On the one hand, the energy present in the truncated series is lower than that of the original flow. On the other hand, due to the truncation, dissipation is under-represented compared with its experimental value and therefore it leads the energy to be larger than it should. The Heisenberg model, which represents the mean action of the small scales, tends to compensate the latter effect so that the solution of the relatively low-dimensional dynamical system can approach the truncated solution of the Navier–Stokes equation and thus mimic the boundary-layer flow. Obviously, it can reach this purpose for one parameter value only. Indeed, large α values will make the energy too small while small α values will make the energy too high. In the 'realistic' model, the energy of each mode should be close to the corresponding eigenvalue. One way to evaluate the best α value is to compute the kinetic energy given by the dynamical system and compare it to that of the original truncated flow. We then define f as the ratio between the energy of the obtained solution and the total energy of the flow, the latter being approximated by considering all the eigenvalues experimentally determined. The curve f versus α (figure 17) in the 32D system shows that the energy decays monotonically with α, which is consistent with our previous discussion, and that f coincides with the original (renormalized) energy content of the truncated flow, namely 0.75, when α is approximately 0.48. (If one wants to recover the total energy of the flow ($f = 1$), α becomes 0.2.)

Second, the coefficients corresponding to a realistic flow field should be uncorrelated (see relation (5)) as the decomposition into orthogonal modes and uncorrelated coefficients is unique. We then define

$$R^{nm}_{kk'} = \left\langle \frac{a^{(n)}_k}{(\lambda^{(n)}_k)^{\frac{1}{2}}} \frac{a^{(m)*}_{k'}}{(\lambda^{(m)}_{k'})^{\frac{1}{2}}} \right\rangle,$$

with $m = n = 1$ for the 32- and 54-dimensional systems. If (5) is satisfied, $R^{11}_{kk'} = R_{kk'}$ is the identity matrix. When α equals the above values, $R_{kk'}$ is indeed very close to a diagonal matrix, the largest non-diagonal element being on the order of 10^{-2}.

It is interesting to note that the corresponding solutions belong to the fourth

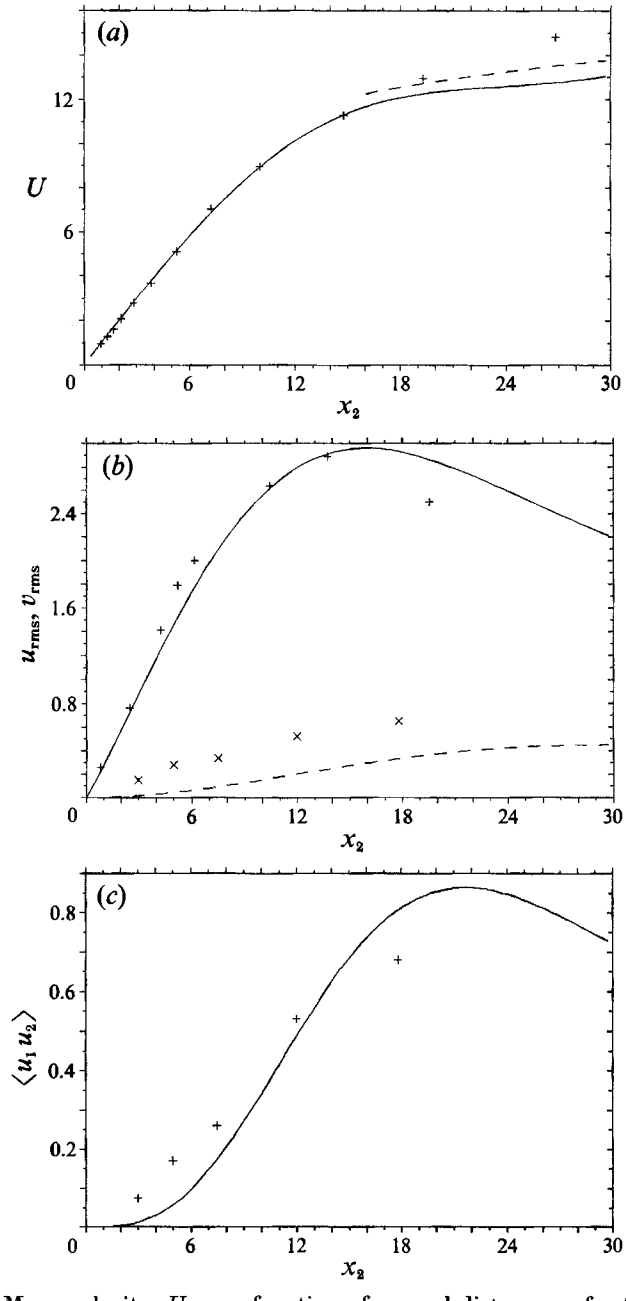

FIGURE 18. (*a*) Mean velocity, U, as a function of normal distance x_2 for the 32D system at the parameter value $\alpha = 0.2$. The dashed line represents the log profile $U = (1/\kappa)\ln x_2 + B$ with $\kappa = 0.41$ and $B = 5.5$ (Sreenivasan 1989). (*b*) Root mean square (streamwise and normal) velocity fluctuations as a function of wall distance x_2 for the same solution as (*a*). Solid line: r.m.s. of u_1, dashed line: r.m.s. of u_2. (*c*) Distribution of $\langle u_1 u_2 \rangle$ as a function of x_2 for the same solution as (*a*). Symbols are experimental values from Eckelmann (1974) at $Re = 8200$ (in (*b*) +, r.m.s. of u_1; ×, r.m.s. of u_2).

window of intermittency and that they indeed appear quite realistic, based on qualitative arguments (see our discussion in §6). In this window, the mean velocity profile, the distribution of the root mean square velocity components and the Reynolds shear stress compare fairly well with Eckelmann's experimental results (Eckelmann 1974) (except for the normal velocity which is too low) (figure 18(*a–c*)). In particular, the mean velocity displays a logarithmic region. (All the above averages are both temporal and spatial, i.e. streamwise and spanwise.)

9. Conclusions

The intermittent behaviour reported in Aubry *et al.* (1988) persists when more streamwise and normal modes are added to the dynamical system as it seems to be a generic property of the equations due to their symmetry invariance. Intermittency consists of high-level activity which alternates with more quiescent periods. At realistic values of the Heisenberg parameter, (non-zero) streamwise modes are always active during the bursts and collapse otherwise while spanwise modes are dynamically active at all times. Intermittently, infinitely long flow structures oscillate and suddenly burst downstream, becoming of finite streamwise length. During the bursts, they are convected downstream at the mean velocity value at the top of the layer and their amplitude oscillates rapidly as high frequencies are excited. The flow 'structures' involved in these motions are streamwise rolls, streaks, sweeps, horseshoe vortex lines, and vertical and horizontal shear layers, in good agreement with findings of experimental and numerical studies. In phase space, intermittency is due to orbits close to heteroclinic or homoclinic cycles connecting complex hyperbolic limit sets. It is interesting to note that our findings, clearly, do not depend on the specific resolution chosen: results of 32D and 54D models, including two and three (positive) streamwise modes are very similar: the basic intermittency, as described above, is present in both models and the instability is due to a Hopf bifurcation with a four-dimensional unstable manifold. The extra modes in the 54D model participate in bursting through a nonlinear instability process, as would higher-order modes in finer resolutions. The influence of higher normal modes, studied in a 64D model, alters only the basic quiescent state which is then a combination of these modes (in physical space, the basic rolls are still present). Again, intermittent events still occur and remain of the same nature.

When streamwise modes are involved, the connecting orbits in the space–time domain represent quasi-travelling waves. Although it is not clear which part of the symmetry group $SO(2) \times O(2)$ is directly involved in the (non-trivial) saddle–saddle connection, the streamwise $SO(2)$ group certainly plays an important role. A theoretical study of this dynamical system structure may lead to a better understanding of spatio–temporal chaos as observed in open flow systems. A similar intermittency has been indeed observed in some solutions of the Kuramoto–Sivashinsky equation in a 'spatio-temporal chaotic regime', so named by Hyman *et al.* (1986). There also, as shown by Aubry & Lian (1992*a*), non-trivial limit sets are connected by quasi-travelling waves.

We would like to thank John Lumley and Philip Holmes for their continuous support and discussions. This work was financially supported by a NSF/PYI award MSS89-57462, a Petroleum Research Grant ACS-PRF no. 23009-G7 and PSC-CUNY grants. Computer resources were provided by the City University of New York, University Computer Center.

Appendix A. Equations for the coefficients of the ODEs

$$b_k^{(n)(m)} = (L_1 L_3)^{\frac{1}{2}}\Bigg[(l^2+k^2)\,\delta_{mn} + \int_0^{X_2}\left\{\mathrm{D}^2\phi_{i_k}^{(m)}\,\phi_{i_k}^{(n)*} - \left(1-\frac{x_2}{H}\right)\phi_{2_k}^{(m)}\,\phi_{1_k}^{(n)*} - \mathrm{i}lx_2\left(1-\frac{x_2}{2H}\right)\phi_{i_k}^{(m)}\,\phi_{i_k}^{(n)*}\right\}\mathrm{d}x_2\Bigg],$$

$$c_{kk'}^{(n)(p)(q)} = -(1-\delta_{k0})\int_0^{X_2}\phi_{j_{k'}}^{(p)}\,\Omega_{k_j-k_j}\,\phi_{i_{k-k'}}^{(q)}\,\phi_{i_k}^{(n)*}\,\mathrm{d}x_2,$$

$$d_{kk'}^{(n)(p)(q)(r)} = \frac{-1}{(L_1 L_3)^{\frac{1}{2}}}\left(\int_0^{X_2}\phi_{1_{k'}}^{(p)}\,\phi_{2_{k'}}^{(q)*}\,\phi_{1_k}^{(n)*}\,\phi_{2_k}^{(r)}\,\mathrm{d}x_2 + \mathrm{i}l\int_0^{X_2}\phi_{i_k}^{(n)*}\,\phi_{i_k}^{(r)}\left\{\int_0^{x_2}\phi_{1_{k'}}^{(p)}\,\phi_{2_{k'}}^{(q)*}\,\mathrm{d}x_{2'}\right\}\mathrm{d}x_2\right).$$

Here, i is the complex number, $\sqrt{-1}$. D denotes the derivative operator with respect to x_2: $\mathrm{D} = \mathrm{d}/\mathrm{d}x_2$. $\boldsymbol{k}$ denotes the wavenumber (l, k), and $\Omega_{k_j} = \mathrm{i}k_j$ if $j = 1, 3$ or $= \mathrm{D}$ if $j = 2$.

Appendix B. Selected eigenvalues of the 32-dimensional system linearized about a fixed point for different subsystems

α	Eigenvalues of the subsystem ($\mathrm{Im}\,(a_{01})$, $\mathrm{Im}\,(a_{03})$, $\mathrm{Im}\,(a_{05})$)		
1.50	−37.336	−4.694	0.004
1.40	−33.640	−3.731	0.453
1.30	−29.876	−2.654	0.420
1.20	−26.042	−0.987	−0.321
1.10	−22.156	(−0.216,	1.476)
1.00	−18.287	(0.221,	2.089)

α	Eigenvalues of the subsystem (a_{-11}, a_{-13}, a_{-15}, a_{11}, a_{13} and a_{15})					
0.95	(−43, 123)	(−41, 71)	(−32, 106)	(−32, 100)	(−14, 65)	(−0.53, 90)
0.90	(−40, 120)	(−38, 68)	(−30, 98)	(−30, 104)	(−14, 62)	(0.41, 88)
0.89	(−40, 119)	(−38, 68)	(−30, 97)	(−29, 103)	(−13, 61)	(0.58, 88)

(a, b) denotes the complex conjugate pair $a+\mathrm{i}b, a-\mathrm{i}b$.

Appendix C. Selected eigenvalues of the 54-dimensional system linearized about a fixed point for different subsysems

α	Eigenvalues of the subsystem ($\mathrm{Im}\,(a_{01})$, $\mathrm{Im}\,(a_{03})$, $\mathrm{Im}\,(a_{05})$)		
2.10	−36.671	−4.672	−0.164
2.00	−34.062	−3.973	0.110
1.90	−31.420	−3.221	0.143
1.85	−30.085	−2.804	0.087
1.75	−27.389	−1.749	−0.288
1.65	−24.659	(−0.695,	1.032)
1.55	−21.909	(−0.382,	1.630)
1.45	−19.164	(−0.069,	2.047)
1.40	−17.810	(0.091,	2.219)

α	Eigenvalues of the subsystem ($a_{-11}, a_{-13}, a_{-15}, a_{11}, a_{13}$ and a_{15})					
1.25	(−39, 125)	(−38, 69)	(−30, 104)	(−29, 110)	(−14, 68)	(−0.17, 95)
1.22	(−38, 124)	(−37, 68)	(−29, 103)	(−27, 109)	(−14, 67)	(0.20, 94)
1.21	(−38, 124)	(−36, 68)	(−29, 103)	(−27, 109)	(−14, 66)	(0.32, 94)

(a, b) denotes the complex conjugate pair $a+ib, a-ib$.

REFERENCES

Adrian, R. J., Moin, P. & Moser, R. D. 1987 Stochastic estimation of conditional eddies in turbulent channel flow. In *Proc. 1987 Summer Program of Center for Turbulence Research. NASA Ames/Stanford University*, pp. 7–19.

Armbruster, D., Guckenheimer, J. & Holmes, P. 1988 Heteroclinic cycles and modulated travelling waves in systems with $O(2)$ symmetry. *Physica* **29D**, 257–282.

Aubry, N. 1987 A dynamical system/coherent structure approach to the fully developed turbulent wall layer. Ph.D. thesis, Cornell University.

Aubry, N. 1991 On the hidden beauty of the proper orthogonal decomposition. *Theor. Comput. Fluid Dyn.* **2**, 339–352.

Aubry, N., Guyonnet, R. & Lima, R. 1991 Spatio-temporal analysis of complex signals: Theory and applications. *J. Statist. Phys.* **64**, 683–739.

Aubry, N., Guyonnet, R. & Lima, R. 1992*a* Spatio-temporal symmetries and bifurcations via biorthogonal decompositions. *J. Nonlinear Sci.* **2**, 183–215.

Aubry, N., Guyonnet, R. & Lima, R. 1992*b* Turbulence spectra. *J. Statist. Phys.* **67**, 203–228.

Aubry, N., Holmes, P., Lumley, J. L. & Stone, E. 1988 The dynamics of coherent structures in the wall region of a turbulent boundary layer. *J. Fluid Mech.* **192**, 115–173.

Aubry, N. & Lian, W. Y. 1992*a* Exploiting and detecting space-time symmetries. In *Exploiting Symmetries in Applied and Numerical Analysis*. Lectures in Applied Mathematics (ed. E. Allgower, K. Georg & R. Miranda).

Aubry, N. & Lian, W. Y. 1992*b* Spatio-temporal structure of compressible turbulence. *Levich Inst. Preprint* 9206022. *J. Statist. Phys.* (submitted).

Aubry, N., Lian, W. Y. & Titi, E. S. 1993 Preserving symmetries in the proper orthogonal decomposition. *SIAM J. Statist. Sci. Comput.* **14**, (in press).

Aubry, N. & Sanghi, S. 1989 Streamwise and spanwise dynamics in the turbulent wall layer. In *Chaotic Dynamics in Fluid Mechanics, Proc. 3rd Joint ASCE-ASME Mechanics Conf., UCSD, La Jolla, July 9–12, 1989* (ed. K. N. & U. Ghia), pp. 110–118. ASME.

Aubry, N. & Sanghi, S. 1991 Bifurcations and bursting of streaks in the turbulent wall layer. In *Turbulence and Coherent Structures, Proc. Grenoble Conf.* on *Organized Structures and Turbulence in Fluid Mechanics, 18–21 September, 1989* (ed. O. Métais & M. Lesieur), pp. 227–251. Kluwer.

Bakewell, P. & Lumley, J. L. 1967 Viscous sublayer and adjacent wall region in turbulent pipe flow. *Phys. Fluids* **10**, 1880–1889.

Berkooz, G., Holmes, P. J. & Lumley, J. L. 1991 Intermittent dynamics in simple models of the turbulent wall layer. *J. Fluid Mech.* **230**, 75–95.

Berkooz, G., Holmes, P., Lumley, J. L., Aubry, N. & Stone, E. 1992 Observations regarding "Coherence and chaos in a model of turbulent boundary layer" by X. Zhou and L. Sirovich. *Phys. Fluids* A (submitted).

Blackwelder, R. F. & Eckelman, H. 1979 Streamwise vortices associated with the bursting phenomenon. *J. Fluid Mech.* **94**, 577–594.

Blackwelder, R. F. & Swearingen, J. D. 1990 The role of inflectional velocity profiles in wall bounded flows. In *Near Wall Turbulence* (ed. S. J. Kline & N. H. Afgan), pp. 268–288. Hemisphere

Bogard, D. G. & Tiederman, W. G. 1986 Burst detection with single point velocity measurements. *J. Fluid Mech.* **162**, 389–413.

Bogard, D. G. & Tiederman, W. G. 1987 Characteristics of ejections in turbulent channel flow. *J. Fluid Mech.* **179**, 1–19.

BUSSE, F. M. & HEIKES, K. E. 1980 Convection in a rotating layer: a simple case of turbulence. *Science* **208**, 173–175.

CAMPBELL, S. & HOLMES, P. 1991 Bifurcation from $O(2)$ symmetric heteroclinic cycles with three interacting modes. *Nonlinearity* **4**, 697–726.

CANTWELL, B. J. 1981 Organized motion in turbulent flow. *Ann. Rev. Fluid Mech.* **13**, 457–515.

CORINO, E. R. & BRODKEY, R. S. 1969 A visual investigation of the wall region in turbulent flow. *J. Fluid Mech.* **37**, 1–30.

CURRY, J. H. 1978 Generalized Lorenz systems. *Commun. Math. Phys.* **60**, 193–204.

CURRY, J. H., HERRING, J. R., LONCARIC, J. & ORSZAG, S. A. 1984 Order and disorder in two- and three-dimensional Bénard convection. *J. Fluid Mech.* **147**, 1–38.

ECKELMANN, H. 1974 The structure of the viscous sublayer and the adjacent wall region in a turbulent channel flow. *J. Fluid Mech.* **65**, 439–59.

GUCKENHEIMER, J. & HOLMES, P. 1983 *Nonlinear Oscillations, Dynamical Systems and Bifurcations of Vector Fields*. Springer.

GUCKENHEIMER, J. & HOLMES, P. 1988 Structurally stable heteroclinic cycles. *Math. Proc. Camb. Phil. Soc.* **103**, 189–192.

GUPTA, A. K., LAUFER, J. & KAPLAN, R. E. 1971 Spatial structure in the viscous sublayer. *J. Fluid Mech.* **50**, 493–512.

HEAD, M. R. & BANDYOPADHYAY, P. 1981 New aspects of turbulent boundary layer structure. *J. Fluid Mech.* **107**, 297–338.

HERZOG, S. 1986 The large scale structure in the near-wall region of turbulent pipe flow. Ph.D. thesis, Cornell University.

HYMAN, J. M., NICOLAENKO, B. & ZALESKI, S. 1986 Order and complexity in the Kuramoto–Sivashinsky model of weakly turbulent interfaces. *Physica* **23D**, 265–292.

JIMENEZ, J. & MOIN, P. 1990 A minimal flow unit in near wall turbulence. *Centre for turbulence research, Stanford University, CTR Manuscript* 105.

JIMENEZ, J., MOIN, P., MOSER, R. & KEEFE, L. 1988 Ejection mechanisms in the sublayer of a turbulent channel. *Phys. Fluids* **31**, 1311–1313.

JOHANSSON, A. V., ALFREDSSON, P. H. & ECKELMANN, H. 1987 On the evolution of shear layer structures in near-wall turbulence. In *Advances in Turbulence*, pp. 383–390. Springer.

KEEFE, L., MOIN, P. & KIM, J. 1987 The dimension of an attractor in turbulent Poiseuille flow. *Bull. Am. Phys. Soc.* **32**, 2026.

KIM, J. 1985 Turbulence structures associated with the bursting event. *Phys. Fluids* **28**, 52–58.

KIM, J. 1987 Evolution of a vortical structure associated with the bursting event in a channel flow. In *Turbulent Shear Flows 5*, pp. 221–233. Springer.

KIM, H. T., KLINE, S. J. & REYNOLDS, W. C. 1971 The production of turbulence near a smooth wall in a turbulent boundary layer. *J. Fluid Mech.* **50**, 133–160.

KIM, J. & MOIN, P. 1986 The structure of vorticity field in turbulent channel flow. Part 2. Study of ensemble-averaged fields. *J. Fluid Mech.* **162**, 339–363.

KIM, J., MOIN, P. & MOSER, R. D. 1987 Turbulence statistics in fully developed channel flow at low Reynolds number. *J. Fluid Mech.* **30**, 741–773.

KLINE, S. J., REYNOLDS, W. C., SCHRAUB, F. A. & RUNSTADLER, P. W. 1967 The structure of turbulent boundary layers. *J. Fluid Mech.* **30**, 741–773.

KLINE, S. J. & ROBINSON, S. K. 1990 Quasi-coherent structures in the turbulent boundary layer: Part I. Status report on a community-wide summary of the data. In *Near Wall Turbulence* (ed. S. J. Kline & N. H. Afgan), pp. 200–217. Hemisphere.

KREPLIN, H. P. & ECKELMANN, H. 1979 Propagation of perturbations in the viscous sublayer and adjacent wall region. *J. Fluid Mech.* **95**, 305–322.

LANDAHL, M. 1990 On sublayer streaks. *J. Fluid Mech.* **212**, 593–614.

LEIBOVICH, S. & MAHALOV, A. 1993 Resonant interactions in rotating pipe flow. *Sibley School of Mechanical and Aerospace Engineering, Cornell University Preprint.*

LOÈVE, M. 1955 *Probability Theory*. Van Nostrand.

LUMLEY, J. L. 1967 The structure of inhomogeneous turbulent flows. In *Atmospheric Turbulence*

and Radio Wave Propagation (ed. A. M. Yaglom & V. I. Tatarski), pp. 166–178. Moscow: Nauka.

LUMLEY, J. L. 1970 *Stochastic Tools in Turbulence*. Academic.

LUMLEY, J. L. 1981 Coherent structures in turbulence. In *Transition and Turbulence* (ed. R. E. Meyer), pp. 215–242. Academic.

MOFFATT, H. K. 1990 Fixed points of turbulent dynamical systems and suppression of nonlinearity. In *Whither Turbulence: Turbulence at the Crossroads* (ed. J. L. Lumley). Lecture Notes in Physics, vol. 357, pp. 250–257. Springer.

MOIN, P. & KIM, J. 1982 Numerical investigation of turbulent channel flow. *J. Fluid Mech.* **118**, 341–377.

MOIN, P. & MOSER, R. D. 1989 Characteristic-eddy decomposition of turbulence in a channel. *J. Fluid Mech.* **200**, 471–509.

MULLIN, T. & DARBYSHIRE, A. G. 1989 Intermittency in a rotating annular flow. *Europhys. Lett.* **9**, 669–673.

NEWELL, A. C., RAND, D. A. & RUSSELL, D. 1988 Turbulent transport and the random occurrence of coherent events. *Physica* **33D**, 281–303.

NICOLAENKO, B. & SHE, Z. S. 1990 Symmetry breaking homoclinic chaos in the Kolmogorov flow. In *Topological Fluid Mechanics* (ed. H. K. Moffatt & A. T. Sinober). Cambridge University Press.

PROCTOR, M. R. E. & JONES, C. 1988 The interaction of two spatially resonant patterns in thermal convection. Part 1. Exact 1:2 resonance. *J. Fluid Mech.* **188**, 301–335.

ROBINSON, S. K. 1991 Coherent motions in the turbulent boundary layers. *Ann. Rev. Fluid Mech.* **23**, 601–639.

ROBINSON, S. K., KLINE, S. J. & SPALART, P. R. 1990 Quasi-coherent structures in the turbulent boundary layer: Part II. Verification and new information from a numerically simulated flat-plate layer. In *Near Wall Turbulence* (ed. S. J. Kline & N. H. Afgan), pp. 218–247. Hemisphere.

SANGHI, S. & AUBRY, N. 1991 Models for the structure and dynamics of near wall turbulence. In *Studies in Turbulence* (ed. T. B. Gatsky, S. Sarkar & C. G. Speziale), pp. 190–206. Springer.

SIROVICH, L. 1987 Turbulence and the dynamics of coherent structures: I, II, III. *Q. Appl. Maths* **5**, 561–590.

SIROVICH, L., BALL, K. S. & KEEFE, L. R. 1990 Plane waves and structures in turbulent channel flow. *Phys. Fluids* A**2**, 2217–2226.

SLIMANI, S., AUBRY, N., KOLODNER, P. & LIMA, R. 1992 Application of biorthogonal decomposition techniques to dispersive chaos in binary fluid convection. In *Bifurcation Phenomena and Chaos in Thermal Convection* (ed. H. H. Bau, L. Bertram & S. A. Korpela), pp. 39–46. ASME.

SMITH, C. R. & METZLER, S. P. 1983 The characteristics of low-speed streaks in the near-wall region of a turbulent boundary layer. *J. Fluid Mech.* **129**, 27–54.

SMITH, C. R. & SCHWARZ, S. P. 1983 Observation of streamwise rotation in the near-wall region of a turbulent boundary layer. *Phys. Fluids* **26**, 641–652.

SPALART, P. R. 1988 Direct simulation of a turbulent boundary layer up to $R_\theta = 1410$. *J. Fluid Mech.* **187**, 61–98.

SREENIVASAN, K. R. 1989 The turbulent boundary layer. In *Frontiers in Experimental Fluid Mechanics* (ed. M. Gad-el-Hak), pp. 159–205. Springer.

STONE, E. & HOLMES, P. 1989 Noise induced intermittency in a model of a turbulent boundary layer. *Physica* **37D**, 20–32.

STONE, E. & HOLMES, P. 1990 Random perturbation of heteroclinic attractors. *SIAM J. Appl. Maths* **50**, 726–743.

THEODERSEN, T. 1952 Mechanism of turbulence. In *Proc. 2nd Midwestern Conf. on Fluid Mech. Ohio State University, Colombus, Ohio.*

WILLMARTH, W. W. & BOGAR, T. J. 1977 Survey and new measurements of turbulent structure near a wall. *Phys. Fluids Suppl.* **20**, S9–21.

WILLMARTH, W. W. & LU, S. S. 1972 Structure of the Reynolds stress near the wall. *J. Fluid Mech.* **55**, 65–92.

ZHOU, X. & SIROVICH, L. 1992 Coherence and chaos in a model of turbulent boundary layer. *Center for Fluid Mechanics Rep.* 91-233. Brown University, RI. Also *Phys. Fluids* (submitted).